Journal Pre-proofs

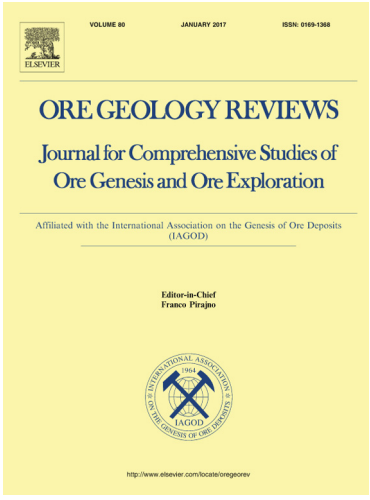

Mineralogical variation in platinum group element within altered chromitite of the Kondapalli Layered Igneous Complex (Southern India): implication on magmatic evolution and its petrogenetic significance

Tushar Meshram

PII: S0169-1368(19)30232-X
DOI: https://doi.org/10.1016/j.oregeorev.2020.103398
Reference: OREGEO 103398

To appear in: *Ore Geology Reviews*

Received Date: 13 March 2019
Revised Date: 24 January 2020
Accepted Date: 9 February 2020

Please cite this article as: T. Meshram, Mineralogical variation in platinum group element within altered chromitite of the Kondapalli Layered Igneous Complex (Southern India): implication on magmatic evolution and its petrogenetic significance, *Ore Geology Reviews* (2020), doi: https://doi.org/10.1016/j.oregeorev.2020.103398

Full title: Mineralogical variation in platinum group element within altered chromitite of the Kondapalli Layered Igneous Complex (Southern India): implication on magmatic evolution and its petrogenetic significance

Author: Tushar Meshram

Affiliations: Geological Survey of India, Central Region, Nagpur, India

Complete contact information for the corresponding author: Regional Petrology Laboratory, Geological Survey of India, Central Region, Seminary Hills, Nagpur-440006, Maharashtra, India

Mob No: +91 9573058434

E-mail Id: tusharmeshram1984@gmail.com

1. Introduction:

Platinum Group Minerals (PGMs) associated with Chromite form in a wide range of geotectonic settings, namely, (1) stratiform or layered magmatic complexes, (2) podiform complexes in ophiolites, (3) the Alaskan zoned complexes and (4) Chromite-rich Archean complexes are also called 'conduit-type' (Mondal and Baidya, 1997; Auge et al., 2002; Ahmed and Arai, 2003; Economou-Eliopoulos, 2010; Mukherjee et al., 2012; Mungall, 2014; Peck and Huminicki, 2016; O'Driscoll and González-Jimenez, 2016; Prichard et al., 2017a-b; Mondal et al., 2019). They may also form as a result of hydrothermal remobilization and may occur as placers. Economic deposits of platinum-group elements (PGEs) in mafic-ultramafic layered intrusions that are derived mainly from basaltic magmas are commonly referred to as PGE-reefs and are the primary hosts of the world's significant PGE resources (Scoates and Friedman, 2008; Mungall and Naldrett, 2008; Naldrett et al., 2008; Peck and Huminicki, 2016; Barnes and Ripley, 2016; Day et al., 2008; O'Driscoll et al., 2009).

The key factors responsible for the formation of large and super-large magmatic sulfide deposits (Ni-Cu-PGE) are (1) large volumes of mantle-derived mafic-ultramafic magmas that are participated in the formation of the deposits; (2) fractional crystallization and crustal contamination, particularly the input of sulfur from crustal rocks, resulting in sulfur saturation and immiscibility and segregation metal-sulfide liquid; and (3) the timing of sulfide concentration in the intrusion (Song et al., 2011). PGE associated with Ni-Cu sulfides in magmatic rocks are also classified into two major groups, (a) Komatiite-related sulfide-rich deposits (>10% sulfide), which are formed due to interaction of mantle-derived magma within the crust that gave rise to the early sulfide immiscibility and (b) stratiform layers (reefs) of large intrusions, e.g., the Bushveld Complex, South Africa, which are generally sulfide poor (<5% sulfide). Earlier it was divided into Ni-Cu-PGE and Ni-Cu-(Co) deposits (Lesher and Keays, 2002; Seabrook et al., 2004; Naldrett et al., 2008; Naldrett, 2010; Song et al., 2011; O'Driscoll and González-Jimenez, 2016; Lu et al., 2019).

The detailed study of Chromite-PGM assemblages can provide evidence or information on the physicochemical condition of the parental melts, their mantle source, formation and entrapment of PGM during Chromite crystallization (Naldrett et al., 2008; Economou-Eliopoulos, 2010; Kapsiotis et al., 2010; Mondal, 2011; Page et al., 2012; Page and Barnes, 2016, O'Driscoll and González-Jimenez, 2016, Zaccarini et al., 2018). It also helps to understand the nature of Ni-Cu-PGE magmatic system (Vuorelainen et al., 1982; Piña et al., 2008, 2012; Song et al., 2011; Prichard et al., 2013; Marchetto, 1990; De Almeida et al., 2007; Gervilla and Kojonen, 2002; Lu et al., 2019). Similarly, the PGM assemblages that begin to deposit at high-temperature parageneses also provide the information regarding their modified composition as result of subsequent late-stage (metasomatic) alteration, metamorphism, low-temperature hydrothermal alteration or surficial weathering (Hudson and Donaldson, 1984; Ballhaus and Ryan, 1995; Hanley, 2005; Marchetto, 1990; De Almeida et al., 2007; Chaumba, 2018; Shcheka et al., 2004; Djon and Barnes, 2012; Suárez et al., 2010; Holwell et al., 2017). The present study deals with such changes in the PGM and Chromite in host chromitites from the Kondapalli Layered Igneous Complex (KLIC) in Southern India.

The KLIC represents a layered igneous complex intruded within the granulite litho ensemble of the Proterozoic Eastern Ghats Belt (EGB) (Leelanandam, 1997). Mineral chemistry of Chromite and the presence of PGMs in the chromitites of the KLIC were documented during an earlier study (Meshram et al., 2014, 2015). The new EPMA data are generated during the present study from the Chromite core and rim with associated PGMs to known the compositional variation during magmatic evolution. The present investigation

aims at inferring the possible source of parental melt and also its primary magmatic characteristics and subsequent hydrothermal or metamorphic evolution based on their nature of distribution, the textural variation, and mineralogical compositional changes of Chromite, PGMs, and associated sulfides. An attempt also made to understand the role of the Ni-Cu-PGE magmatic system during the evolution of KLIC, which classifies and characterizes the mineralization style and helps for further exploration.

2. Geological Setting of the KLIC

The rocks of KLIC intruded within the Eastern Ghat Belt (EGB) are complex in terms of lithological setting and tectonothermal history (Leelanandam and Vijaya Kumar, 2007; Meshram et al., 2014, 2015). The litho-variants are mainly felsic and mafic granulites, metapelites, a layered complex, and intrusive mafic dikes occur in the area (Leelanandam, 1972, 1997; Nanda and Natarajan, 1980; Leelanandam and Vijaya Kumar, 2007; Fig. 1). The KLIC is representing 1.7 Ga magmatism in the area, which is subsequently affected by the prolonged polyphase granulitic facies metamorphism between 1.65 and 1.55 Ga (Mezger and Cosca, 1999; Kovach et al., 2001). This 1.7 Ga magmatic event of KLIC is correlated with the accretion of the Napier complex to Proto-India (Dobmeier and Raith, 2003; Dharma Rao et al., 2004), and also related to the formation of the Columbia supercontinent (Rogers and Santosh, 2002, 2004; Dharma Rao and Santosh, 2011; Dharma Rao et al., 2012). Nanda and Natarajan (1980) recorded the brecciation and pull-apart structure in the Chromite grains indicating post-emplacement deformational features, which is followed by the overprints of terminal phases of granulite facies metamorphism of the EGMB over the rocks of KLIC. The second phase of rift-related magmatism took place between 1.4 and 1.2 Ga (Upadhyay et al., 2006; Vijaya Kumar et al., 2007). All the litho units might have experienced Pan-African overprints (Upadhyay et al., 2006).

The KLIC occurs as discontinuously disposed and dismembered layered mafic and chromiferous ultramafic rocks within-host high-grade metamorphic rocks, i.e., charnockite, pyroxenite granulites (Leelanandam, 1972, 1997; Nanda and Natarajan, 1980). The mafic members comprising gabbroic and anorthositic rocks and their variants are spatially associated with subordinate ultramafic members, eg., dunite, harzburgite, websterite, orthopyroxenite, clinopyroxenite and orthopyroxene chromitite (Nanda and Natarajan, 1980, Leelanandam, 2006). The gabbroic and anorthositic rocks show prominent layering, and hence they are designated as the Gabbro-Anorthosite Layered Series; the chromitites and ultramafic rocks (which show weak layering and which characteristically contain

disseminated Chromite) constitute the Chromitite-Ultramafic Rock Series (Leelanandam, 1999); however, chromitite-orthopyroxenite/clinopyroxenite banding is rather common. Orthopyroxenite is the most common ultramafic member in the Chromitite-Ultramafic Rock Series of the KLIC (Leelanandam and Vijaya Kumar, 2007). It also suggests that the KLIC constitutes the plutonic core of a continental magmatic arc for Gabbro-Anorthosite Layered Series, and the Chromite-bearing ultramafic cumulates of Chromitite-Ultramafic Rock Series from as a part of the arc-root tectonic setting (Leelanandam and Vijaya Kumar, 2007; Dharma Rao and Santosh, 2011; Dharma Rao et al., 2012; Meshram et al., 2014; 2015). Prominent isomodal layering formed by alternating mafic and felsic (plagioclase) rich layers characterizes the gabbroic and anorthositic rocks. The ultramafic rocks including the chromitites, exhibit weak layering mainly formed by Chromite-rich layers alternating with layers of mafic silicate phases (Fig. 2a). The chromitites from KLIC generally display Chromite (>95%) monomineral layering and banding along with ultramafic rocks, especially orthopyroxenite.

The different components of the KLIC occur as isolated sheets, bands, or lenses with the largest ones being about 1km in length and a few hundred meters in width. In which the CURS has a restricted areal distribution and exhibits a discordant relationship with the mafic members, as observed in the Binny's Quarry, Loya Quarry, Nakkerlapadu Quarry, Yedurlakonda Quarry and Gangineni Quarry (Fig. 1). The Chromite bearing ultramafic bodies occur in an *en echelon* pattern as tectonic pods and slices in the limbs of regional folds possibly due to shearing along the axial planes (Fig. 1). The chromitite bodies are discontinuous and with limited strike extension, often are only a few meters thick (Krishna Rao, 1964; Leelanandam, 1967; Krupanidhi and Subrahmanyam, 1969; Chakravarti and Mukherjee, 1971). Chromite occurs as lenses, pods, pockets, bands, and as disseminations within orthopyroxenite (Fig. 2a and 2b). Carbonate veins are often associated with an anastomosing pattern or as fine networking along with microfractures/shears. They are also subjected to hydrothermal alteration producing serpentine and talc (Fig. 2b).

3. Sampling and methodology:

The representative 25 nos. of samples were collected from all quarry sections. The main sampling was done along the exposed quarry sections (Binny's Quarry, Loya Quarry, Nakkerlapadu Quarry, Yedurlakonda Quarry, and Gangineni Quarry) where the Chromite mineralization occurs as fine dissemination, pockets, pods, and layers within fresh and altered ultramafics, i.e., orthopyroxenite. The Chromite ore samples were collected from fresh and

altered host ultramafic rock to know the compositional variation and effect of alteration. All samples were prepared as thin polished sections for petrographic study. The same sections were used for the search of the platinum group of minerals and associated sulfides.

The petrographic studies of Chromite bearing ultramafics were carried out using LEICA DM RX, at Geological Survey of India, Hyderabad, India. The sections were selected for the EPMA study after detailed petrographic studies to know the compositional variation of Chromite and also search for a platinum group of minerals. Both quantitative electron-microprobe analyses with wavelength-dispersion spectrometers (WDS) and energy-dispersion X-ray spectrometry (EDS) were done with a CAMECA SX100 electron microprobe with an accelerating voltage of 15 kV and 2.387e−7˚A beam current, at the EPMA Laboratory, Geological Survey of India, Southern Region, Hyderabad (India). The PGM and sulfides were analyzed with a voltage of 20 kV and a beam current of 20 nA, with a beam 1μm in diameter. The duration of the analyses varied from 10 to 30s

Similarly, oxides and silicates were analyzed on working conditions with15 kV voltage and 12nA beam current. The data were reduced using phi-rho-z correction procedures. SiO_2, TiO_2, Al_2O_3, Cr_2O_3, FeO, MnO, MgO, CaO, Na_2O, and K_2O were analyzed for all samples. Signals used were S: Ka, Ag: Lb, Fe: Ka, Cu: Ka, Co: Ka, Pt: La, Ni: Ka, As: La, Pd: La, Ru: La, Rh: La, Sb: La, Te: La, Os: Lb, Ir: La, Au: La and Bi: Ma. Standardization was done using default samples. The following internal standards were used: S and Fe on pyrite, Ag on Ag, Co on Co, Pt on Pt, Ni on Ni, As on Ga As, Pd on Pd, Ru on Ru, Rh on Rh, Sb on Sb, Te on Te, Os on Os, Ir on Ir, Au on Au and Bi on Bi. Natural standards were used for all elements except Mn and Ti for which synthetic standards were used. The raw analytical data were corrected with a PAP matrix correction program.

4. Result:

4.1. Petrography

The detailed petrographic study of chromitite and pyroxenite suggests that the KLC exhibits overall equilibrium textures formed during a magmatic phase of crystallization at high-temperature and post-cumulus to sub-solidus re-equilibration. The detailed petrographic observations are as follows.

The chromitite is predominantly massive and shows a cumulate texture. Although, disseminated Chromite is common near the contacts with the enclosing pyroxenite. Massive chromitite (>90% Chromite) is monomineralic, which is composed of coarse euhedral

chromian spinel (Fig. 2a and 2e) and occur as band or layers with associated pyroxenites. Banded chromitite consists of layers of chromian spinel (up to 5 cm thickness) and pyroxenite (Fig. 2a). It also exhibits overall equilibrium textures, which formed both during the magmatic phase of crystallization and high-temperature, post-cumulus to sub-solidus re-equilibration. The chromitites shows excellent solid-state textures with regular triple junctions and 120° grain boundaries, typically indicative of high-temperature annealing (Fig. 2e) (Vernon, 2004). Interstitial silicates (olivine, pyroxene) (Fig. 2c) in chromitite have been altered to chlorite and serpentine (Fig. 2d). Chromite grains exhibit variable degrees of alteration on their margins and along with fractures. Fresh Chromite grains are translucent and reddish-brown to orange in polarized light (Fig. 2e), whereas altered grains are opaque.

In contrast, the disseminated chromitite (≤35 to 40% chromian spinel) has smaller and more subhedral crystals of chromian spinel than the massive chromitite, which are mostly associated with serpentinite (Fig. 2c and d). The Chromite also occurs as an inter-cumulus or interstitial phase within pyroxenite. At places, the inclusion of Chromite noticed within pyroxene grains. Most chromitite samples exhibit pull-apart fractures, and late shearing and faulting produced mylonitic and cataclastic textures. The chromian spinel shows ferric Chromite composition due to replacement along with the fracture plane (Fig. 2f).

Chromite rich orthopyroxene is medium to coarse-grained and exhibits commonly an adcumulate texture comprising the euhedral cumulus enstatite (En_{73} to En_{92}) (Fig. 2c), with a small amount of hypersthene, augite, ferrosilite, and pigeonite. Orthopyroxene is a euhedral in shape that contains hornblende and biotite as intercumulus phases. Fine-grained intergranular Chromite occurs as disseminations. Plagioclase is a rare accessory. Samples proximal to shear zones exhibit cataclastic effects, e.g., undulatory extinction, bent cleavage, bent lamellae, and kink bands. Several sulfide phases like pyrite, chalcopyrite, pentlandite, millerite, and pyrrhotite occur interstitial phases to silicate and Chromite in the pyroxenites and chromitites.

4.2. Mineral Chemistry:

Representative Chromite, pyroxene, platinum-group mineral, and base-metal sulfide grains from the KLIC were analyzed. They are included, 29-analysis from fresh Chromite core, 31-analysis from Chromite altered rim, 17-analysis from orthopyroxene, 24-analysis from PGM and 9-analysis from sulfides. In most cases, several analyses were made on

mineral grains, and those analytical compositions with totals close to 100% and a satisfactory structural formula were selected as representative (Tables 1 to 3).

4.2.1. Chromite

The investigated chromitites samples are composed of fresh Chromite grains with an irregular altered rim. The altered Chromite grains are pitted in nature and exhibit an increasing effect of post magmatic alteration towards the grain boundaries or along cracks. Special care was taken to obtain the Chromite core$_{(N-29)}$ composition of fresh Chromite grains. Unaltered core compositions were obtained by Electron-microprobe analyses (EPMA), and the average Chromite core analyses are presented in Table 1. Similarly, some analyses also included the altered Chromite rim$_{(N-31)}$ to show the compositional variation during the alteration (Barnes, 2000; Evans, 2015, 2017). The Chromite core composition of chromitites from KLIC is consistent with the range of primary magmatic crystallization composition (as discussed below).

Chromites in KLIC show core to rim variation due to alteration, their range of Cr_2O_3 varies from 50.54 wt% to 56.63 wt% within fresh core, whereas 44.12 wt% to 49.77 wt% in altered rim; Al_2O_3 contents range from 10.76 wt% to 12.83 wt% in fresh core and 10.83 wt% to 17.02 wt% in altered rim; FeO^t contents range from 21.86 wt% to 28.46 wt% in fresh core whereas 27.34 wt% to 37.99 wt% in altered rim and MgO ranges from 06.52 wt% to 09.55wt% in fresh core, whereas 04.51 wt% to 08.25 wt% in altered rim (Table no.1). The Fe_2O_3 contents range from 02.74 wt% to 06.28 wt% in the fresh core, while 06.22 wt% to 13.62 wt% in the altered rim. Consequently, their Cr# [Cr/(Cr + Al)] shows very narrow range from 0.73 to 0.77 in fresh core and 0.63 to 0.73 in altered rim. The Mg# [Mg/(Mg + Fe^{2+})] ranges from 0.33 to 0.47 in fresh core and 0.24 to 0.40 in altered rim, respectively. The TiO_2 and MnO do not show any significant variation, unlike other oxides. Calculated melt composition of Al_2O_3 and (FeO/MgO) by Maurel and Maurel, (1982) from Chromite core are ranges from 6.38 to 9.88 and 0.56 to 0.89.

4.4.2. Orthopyroxene

Pyroxenes occur as intercumulus phases to Chromite in the chromitites of KLIC. These are Mg-rich with restricted variation in composition and confirm mostly to enstatite and less commonly to clinoenstatite according to the classification by Morimoto (1989), (Fig. 3B) with a general composition of (En_{92-73}). Their MgO contents range from 25.6 wt% to 32.9 wt% and Mg# from 0.74 to 0.92. They exhibit relatively higher contents of Al_2O_3 (0.3–

3.6 wt%), CaO (0.12–0.79 wt%) and FeO (4.8-15.6 wt%), and meager proportions of MnO, TiO_2, and K_2O (Table no 2). The orthopyroxenes are plotted in the Al_2O_3 vs. Mg# binary diagrams represented by a separate cluster for KLIC with SSZ peridotite affinity (Fig. 5c). Leelanandam (1997) suggests that a quite variable composition of orthopyroxene in chromitites (En_{94-85}) and ultramafic rocks (En_{94-62}) is comparable with the present study. However, it is very much restricted in the gabbroic and anorthositic groups (En_{62-51}).

4.2.3. Platinum-group minerals (PGM)

All Chromite samples examined by EPMA were found to contain minute (from 2 μm to 10 μm) inclusions of PGM. Twenty PGM grains were recorded in six polished sections. Nine PGM grains are observed within Chromites in samples GQ-1_{n-7} and GQ-$2_{n-2,}$ which were found to be suitable for analyses for PGE (Fig. 7a-d) (Table 3).

Most of the PGM grains occur as inclusions in Chromite, and their incidence is relatively more in Fe-rich Chromite rims and minor proportion in the unaltered cores. Sulfides were found along with interstitial spaces or fractures between Chromite and silicate grains (Fig. 7e-f). A majority of the identified PGM are members of the laurite (RuS_2)-erlichmanite (OsS_2) solid solution series, followed by members of the irarsite (IrAsS) and osarsite (OsAsS) (Fig. 7 and 8) and minor ones include Ru–Os–Ir–Fe–Ni–(Rh) alloys (Fig.7 and 8). Two paragenetically distinct populations of PGM could be recognized based on the micro-texture and mode of occurrence. These are as follows:-

1) The independent subhedral to anhedral shape laurite and irarsite occur in Chromite core represent as a relict of the primary mineral phase without any sulfides and sulpharsenides association (Fig. 7a-d).

2) The subhedral to euhedral PGM grains comprising As-bearing laurite and erlichmanite, the sulfarsenides irarsite located along Chromite rim and matrix, are suspected to be altered products of primary phases during hydrothermal alteration. Sulfides comprising millerite and pentlandite are mostly fresh and occur as independent grain (Fig. 7f-g).

The laurite shows variation in composition from Ru-rich laurite (Ru:49% to 50.53%, Os:4.27% to 4.89%) to the Os-rich laurite (Os: up to 31.94%, Ru: up to 23.49%) (Fig. 7& 8). They also exhibit a restricted range of variation in Ir: 4.12% to 7.96% and S: 29.57% to 36.17%, respectively. Some laurite grains found inside unaltered Chromite cores display zoning with a decrease in Ru and S contents, while an increase in corresponding Os-Ir-As contents. Similarly, the irarsite also shows the variation in Ir, Ru, Os, As, and S like laurite. Their range varies from Ir-rich irarsite (Ir: 54.82% to 57.77%, As: 22.82% to 25.66%, Os: 1.83% to 2.85%, Ru: 0.42% to 0.66%) to the Ir-poor irarsite (Ir: 26.49% to 40.92%, As:

10.27% to 18.75%, Os:11.61% to 27.89%, Ru:2.22% to 5.38%). Erlichmanite was only present near the boundary of Chromite grain and not shown any major variations in the analysis (Table 3). At Places along Chromite altered or along with fractures, these subhedral to anhedral grains (Fig. 7) show a systematic increase of S and Os contents (Table 3).

The observed sulfide phases include pentlandite and millerite besides native silver and gold (Table 3) are randomly distributed in the chromitites of KLIC. In the chromitites, sulfides account for less than 1 vol% and are common in samples from Loya Quarry-1, Binny Quarry -1, 2, and Nakkerlapadu Quarry -1 (Fig. 7). All these minerals are secondary in origin and occur along with fractures in Fe-rich Chromite and magnetite or as intercumulus phases in chromitites (Fig. 7 e, f, g). These sulfide grains generally range from several μm to 200 μm across. Compositional range of millerite is observed to be: Ni- 41.08% to 64. 04%, S- 28.98% to 38.83%, Fe- 0.31% to 18.04% with minor Pt- 0.034% to 0.34% and of Pentalandite, Ni-41.08%, S- 38.83% and Fe-18.04%. Compositional range of silver shows Ag- 50% to 85% with S,-1.4% to 13.18% and that of gold Au- 97.63% and Fe- 2.53% (see Table 3). They mostly occur as independent grains without any alteration, suggesting their secondary hydrothermal origin.

The binary and ternary variation diagram shows the distribution of PGE and also supports the evolution trend from primary magmatic to secondary alteration (Fig. 8 and 9). The OsS_2-RuS_2-IrS_2 ternary diagram (Fig 8a) shows a solid solution series of laurite to erlichmanite. Similarly, IPGM dominant nature also indicated in Fig 8b, which shows a clear difference in composition between PGM and sulfides. The triangular diagram (Pt + Fe) – (Os + Ru) – (Ir + Rh) of Slansky et al. (1991) are also used to estimate the temperature of the formation of PGMs from KLIC in Fig. 8c. Correspondingly, the binary variation diagrams of Ru vs. Os, Ir, Rh, Pt, Pd, S, and As suggest the changes in PGMs, they are consistent with compositional changes that occur in Chromite core to the rim (Fig. 9).

5. Discussion

5.1. *Characterization of Chromite:*

The composition of the fresh core and altered rim of Chromite plotted in the Cr–Al–Fe^{3+} diagram, which shows Al-Chromite composition for fresh core analysis and samples trend, shows an affinity towards Fe-Chromite for altered rim (Fig. 3a). The binary variation diagram Cr_2O_3 vs. Al_2O_3 and FeO^t shows a perfect negative correlation, suggesting that during hydrothermal alteration and/or metamorphism Al_2O_3 and FeO^t show enrichment from Chromite core to the rim (Fig 3 c and d). which is consistent with the effect of high-

temperature post-cumulus stage alteration (Leelanadan, 1997; Barnes, 2000; Barnes and Roeder, 2001; González-Jiménez et al., 2009; Evans, 2015). Although the Chromite has noticeable compositional variations, still they are in a range of primary magmatic field, especially Chromite core. It is also supported by the good inverse correlation between MnO and Mg#, which is an indication that the analyzed Chromites has not suffered significant alterations (Barnes, 2000).

Similarly, the major oxides of the Chromites (Table 1a and 1b) show typical compositional trends relative to the field of layered intrusions in the comprehensive worldwide compilation of Barnes and Roeder (2001) (Fig. 3e and 3f). There is a very limited spread of Mg# (Mg/[Mg+Fe2+]) atomic ratio in percent) and the Cr# (Cr/[Cr+Al] atomic ratio in percent) of Chromite from KLIC and they are considered normal for orthocumulate rocks in tholeiitic layered intrusions (Fig. 3e) (Evans, 2017). TiO_2 is particularly sensitive as an indicator of reaction with late liquids (Roeder and Campbell, 1985), as it can be observed in TiO_2 vs. Fe^{3+}# Chromites plotted, where they are correlated with the 50% global layered intrusions Chromite field and follows usual oxidation liquid reaction trend (Fig. 3f) (Evans, 2017). Evans, (2017) in their study suggest the widest range of minor element variations for the three intrusions (KMKA intrusions in East Africa) of similar tectonic setting shows vast compositional difference due to the variation of assimilation of different contaminant source. Their results are overwhelming the primary compositional range and mislead the tectonic setting in the discriminations diagram. Present study has indicated that TiO_2 of Chromite core has limited range from 0.17 wt% to 0.32 wt%, which are within the range of boninites-arc tholeiites (<0.35 wt%) (Kamenetsky et al., 2001) and not show wide range (up to 5 wt%) due to assimilation and crustal contamination as suggested by Evans, (2017). The reported range of TiO_2 composition from the Chromite core is indicative of primary magmatic crystallization signature as suggested by Barnes (2000); Barnes & Roeder (2001) and Kamenetsky et al., (2001). Therefore, TiO_2 from Chromite core can be used to understand the tectonic setting of KLIC, which is discussed in detail under the next section.

Subsequently, KLIC Chromite composition are also compared with the Cr–Al–Fe^{3+} compositions of spinels from different metamorphic facies (Purvis et al., 1972; Evans and Frost, 1975; Suita, and Strieder, 1996) (Figure 5a), as well as with spinel stability limits (Sack and Ghiorso, 1991; Barnes, 2000), most of them are comprised in the field of spinel metamorphosed in the upper greenschist facies, at temperatures ranging from 500°C to 550 °C, whereas, some of the altered rim samples are shown an affinity towards the lower amphibolite facies spinel field.

The range of temperature, i.e., 500°C to 550°C, is considered as a primary magmatic composition rather than post-magmatic alteration (Barnes, 2000). Barnes (2000) further suggested that these primary greenschist facies Chromite compositions, on the other hand, imply higher equilibration temperatures in the range from 1400°C to 750°C, which is apparent paradox that can be explained if the 'primary greenschist' compositions are relics of the original igneous cooling stage, and have not been substantially reset during metamorphism or alteration. The calculated melt composition of Al_2O_3 and (FeO/MgO) by Maurel and Maurel (1982) also supported its similarity with primary boninite/tholeiite melt composition. These indicate that the Chromite cores were not affected by post-magmatic re-equilibration, and therefore preserve their primary compositions.

Furthermore, the calculated crystallization temperature of orthopyroxene by Fe and Mg mole fractions were plotted in an experimentally contoured pyroxene quadrilateral (pyroxene-solvus thermometer of Lindsley, 1983) at 1.0 GPa indicating 1300-1250°C, which is interpreted as the igneous crystallization temperature of the residual mantle also support their original primary nature of Chromite core (Lindsley, 1983; Ishwar-Kumar et al., 2016a-b). These above observations suggest that the Chromite core has still preserved primary igneous crystallization signatures, which can be further used for characterization of source and to know their geodynamic setting.

5.2. ***Nature of magma source and tectonic setting:***

We used the mineral chemistry of the Chromite to determine the parental melt composition because its composition is strongly related to its parental melt composition, the degree of partial melting, and its fractional crystallization (Irvine, 1977; Dick & Bullen, 1984; Barnes and Roeder, 2001).

The ultramafic cumulates of the KLIC occur as small lenses, and bands show the primary layering, which is mainly represented by Chromite-pyroxenite banding (Fig. 2a). Cumulate textures are well preserved throughout the KLIC, and adcumulus growth was the dominant form of post-cumulus enlargement. The Chromite core analysis is used to know the nature of parental magma and tectonic setting, as they are least affected and consistent with primary magmatic characteristics.

The Al_2O_3 content of Chromite is commonly used to determine the nature of its parental melt and its ambient tectonomagmatic environment (e.g., Zhou et al., 1996; Kamenetsky et al., 2001; Rollinson, 2008; Zaccarini et al., 2011). Similarly, calculated the Al_2O_3 contents of melts in equilibrium with Chromite (equilibrium at 1 kbar) using the

equation: Al_2O_3, $_{spinel}$ =0.035×(Al_2O_3, $_{melt}$)$^{2.42}$ as proposed by Maurel & Maurel (1982). The results indicate that the parental melts through which the KLIC Chromite crystallized had Al_2O_3 contents of 06.38–09.88 wt% (Table 1a). Such high Al_2O_3 contents are representative of boninitic melts (Wilson, 1989), so the parental melts of the KLIC Chromite bearing ultramafic had an arc parentage (Fig. 6a-6d).

Consequently, the ranges of Cr# (Cr number) and TiO_2 of Chromite from the KLIC chromitites are similar to island arc boninitic and tholeiitic series peridotites (Fig. 6b-6c) (Kamenetsky et al., 2001). Their enrichment of Fe and Al in the Chromites from KLIC may be explained in number of ways, i.e., (a) the crystal fractionation and/or assimilation processes in parental magmas that led to their more Fe- and Al-rich end compositions (Barnes & Roeder, 2001), or (b) more likely because of reactions between cumulus Chromite and the evolved trapped liquid (Roeder and Campbell, 1985; Leelananda1 and Vijaya Kumar, 2007). In the Cr# vs. TiO_2 diagram (after Choi et al. 2008), Chromite plots with slight variation in TiO_2 at constant Cr# in the boninite field (Fig. 6b), and it is surmised to be due to higher Fe^{2+}# content and melt-mantle interactions (Fig.5b). The above observations are also have similarity with the Chromite mineral chemistry and whole-rock geochemistry studies carried out by Leelanandam, (2004); Leelanandam and Vijaya Kumar, (2007); Dharma Rao and Santosh, (2011); Meshram et al., (2014, 2015).

The parental melt data, along with the Al_2O_3 contents of Chromite, also plot very close to the evolutionary trend of an arc system in a diagram of Al_2O_3 $_{in\ melt}$ v. Al_2O_3 $_{in\ spinel}$ (Fig. 6d; Kamenetsky et al., 2001; Rollinson, 2008) suggest a major role of partial melting. Besides, the FeO/MgO ratio of a parental melt in equilibrium with Chromite at 1 kbar can also be estimated from a Chromite composition using the equation:

$$\text{In } (FeO/MgO)_{spinel} = 0.47 - 1.07Y_{(spinel,\ Al)} + 0.64Y_{(spinel,\ Fe3+)} + \ln(FeO/MgO)_{liquid}$$

Where FeO and MgO are in wt% and

$Y_{(spinel,\ Al)}$ = Al/(Al+Cr+Fe^{3+}) and $Y_{(spinel,\ Fe3+)}$ = Fe^{3+} /(Al+Cr+Fe^{3+}) as proposed by Maurel and Maurel (1982). The results show that the parental magma from which the Chromite crystallized had a FeO/MgO ratio of 0.56 - 0.89 (Table 1a). Boninites have a FeO/MgO ratio over the range 0.7 - 1.4, whereas the same ratio in MOR basalts varies over 1.2 - 1.6, suggesting the KLIC Chromite had an arc derivation. The parental magma was, Al- and Fe-rich and is comparable to the chemical characteristics of boninites magma. Based on all the above lines of evidence, we suggest that the composition of the parental magma of the KLIC chromitites rocks was similar to that of primitive boninitic /tholeiitic basalt formed by a high degree of partial melting of mantle peridotite.

The chrome spinels have been widely used as petrogenetic indicators. The Cr_2O_3, Al_2O_3, and TiO_2 are the main oxides of spinel/Chromite, which are widely used to discriminate between different magma types, their tectonic affinities, and mantle source. The EPMA data on Chromite cores from KLIC was plotted on the discriminate diagrams to decipher the geodynamic settings. In the Fe^2 / Fe^2 + Mg vs., Cr /Cr+Al (Fig.4 b) diagram they distinctly fall in the field of layered intrusion (Fig. 4a and b), whereas in the $Mg/Mg+Fe^{+2}$ vs. $Fe^{+3}/(Fe^{+3}+Cr+Al)$ diagram Chromite core samples falls along the overlapping fields of Alaskan, ophiolitic and stratiform Chromites field (Fig.4 c). Their layered nature also gets supported by TiO_2 vs. Fe^{+3}# diagram (Fig. 3f) by Barnes and Roeder (2001) and Evans (2017). In the Al_2O_3 vs. TiO_2 discrimination diagram (Pearce et al., 1984, Kamenetsky et al. 2001), Chromites plot in the field of island arc tectonic setting (Fig. 6a). The Chromite rich ultramafic rocks of KLIC exhibit characteristics typical of subduction-related magmatic arc setting. Such tectonic signatures are attributed to the closure of the ocean that led to the formation of the suture zones (e.g., Presence of the Bondla ultramafic-mafic complex, western India within Kumta suture, Ishwar-Kumar et al., 2016b). In such a case, the presence of KLIC in the contact between Eastern Dharwar Craton and Eastern Ghat Granulite Belt represents a part of a relict magmatic arc along the suture.

5.3. *Genesis of PGMs*

The PGE signature of mantle-derived rock is significantly used to track the changes during mantle melting and mobilized or transport and distribution of these elements in natural geological materials (Auge et al., 2002; Ahmed and Arai, 2003; Economou-Eliopoulos, 2010; Peck and Huminicki, 2016; O'Driscoll and González-Jimenez, 2016; Lorand and Luguet, 2016). Recent studies on PGM by high precision micro-beam techniques, such as LA-ICP-MS and EPMA studies suggest their distribution during Chromite crystallization (Pearson et al., 2002; Malitch et al., 2003; Ahmed et al., 2006; Shi et al., 2007; Marchesi et al., 2011, Page, 2016). Arguin et al. (2016) also conducted numerical modelling of IPGE and Rh distribution, which suggest that the Chromite, olivine, and/or PGM all contribute to the distribution of these elements during crystal fractionation of sulfide-undersaturated magmas. The PGMs are occurring as inclusions in growing Chromite grains and also preserved imprints of altered or metamorphism, as well as weathering and lateritization (Hudson and Donaldson, 1984; Bowles, 1986; Marchetto, 1990; Ballhaus and Ryan, 1995; Shcheka et al., 2004; Suárez et al., 2010; Garuti et al., 2012; Aiglsperger et al., 2015; Garuti et al., 1997, 2007; Proenza et al., 2007, 2008; Zaccarini et al., 2005, 2008, 2009; 2016; Hanley, 2005, De

Almeida et al., 2007; Djon and Barnes, 2012; Holwell et al., 2017; Chaumba, 2018;). Particularly, the IPGE+Rh bearing Chromite behaves differently during slow and fast cooling (Page, 2016).

The temperature and sulfur fugacity are the essential parameters that control the precipitation of magmatic Os-, Ir- and Ru-bearing PGM during Chromite crystallization. Laurite generally form an equilibrium with Os–Ir–(Ru) alloys at a temperature around 1250ºC to 1300ºC with relatively low sulfur fugacity as describes in number of experimental studies (Garuti et al., 1999a, 1999b; Uysal et al., 2007; Augé and Johan, 1988; Kapsiotis et al., 2009). Studies also suggested that laurite becomes progressively enriched in Os with decreasing temperature and increasing sulfur fugacity, up to the stability field of erlichmanite (Fig 8a and 8b). The triangular diagram (Pt + Fe) – (Os + Ru) – (Ir + Rh) of Slansky et al. (1991) allowed an estimate of the temperature of formation and was applied to the PGMs of KLIC (Fig. 8c). The composition of multiphase assemblages from the KLIC is plotted with the temperature of formation in Fig. 8c, which shows the highest temperature, up to 800°C for the PGMs occur in the Chromite core; whereas, it shows 850°C and above temperature for the PGMs situated at the Chromite rim. The textural evidence of the multiphase associations of minerals and the interpretation of the compositional data with the help of the diagram of Slansky et al. (1991) point to the high-temperature formation of the Ir–Os–Ru alloy, followed by the metamorphism in the chromitites of KLIC.

The analyzed relict primary laurite and irarsite from the Chromite core generally has a low content of Os than that of the Chromite rim (Fig 9), which indicates that during initial deposition, the sulfur fugacity (fS_2) is well below the Os–OsS_2 buffer (Table.3). In contrast, the crystallizing laurite scavenged Ru from the melt (or Ru from Ru-bearing alloys) with decreasing temperature and increasing fS_2, which promotes the enrichment of Os into the laurite lattice because of the laurite-silicate melt partition coefficient with falling temperature (Brenan and Andrews, 2001) (Fig 8). The existence of primary Ru-rich (and Os–Ir poor, Ni-free) inclusions of PGM indicates an initial (and perhaps long-lived) percolation of S-undersaturated melts, consistent with the origin of the KLIC chromitites under arc setting. The result suggests that Os-Ir-Ru alloys from the KLIC chromitites crystallized at relatively high temperature and low fS_2 condition within an S-undersaturated boninitic magma ascending from the upper mantle where they are trapped by the growing Chromite crystals (similar condition reported recently within chromitites of Sukinda Massif, Orissa, India, Mondal et al., 2019). This episode was followed by an influx of melts or fluids in an open system and a rapid increase of fS_2 that destabilized the presence of alloys and also promoted

the precipitation of IPGE-sulphides and sulfarsenides, which indicates that the PGE mineralogy is sulfide poor with only a few grains of laurite. Arsenic bearing PGMs are present mostly along the cracks suggesting the introduction of As during hydrothermal alteration of the rocks, perhaps during serpentinization event (e.g., Bowles et al., 1994; Prichard et al., 2017; Mondal et al., 2019).

The texture supported by the EPMA study reveals the variation in composition and distribution of Cr_2O_3, Al_2O_3, FeO^t from Chromite core to the rim, and similarly in Os-Ir-Ru-S-As content of PGM due to alteration. As a result, affected Chromite grain shows enrichment of Al_2O_3 and FeO^t content along the rim. Similarly, PGM occurs along the Chromite rim also shows variation, as shown in Fig. 9. The binary variation diagram of Cr_2O_3, against Al_2O_3 and FeO^t (Fig 3 c and d) of Chromite and variation of Ru against Os, Ir, Rh, Pd, Pt, S, and As of PGM reveals the systematic change occurs during the alteration (Fig. 9). The above observations also supported by experimental studies by Brenan and Andrews (2001) and Fonseca et al. (2012), which suggest that Ru, Os, and Ir are retained as alloys and, to a lesser extent, sulfides, at a relatively low sulfur fugacity (fS_2) and high temperature (1200 ºC –1300ºC) conditions. Under such conditions, laurite shows a composition of nearly pure RuS_2 with low concentrations of Os and Ir (Brenan and Andrews, 2001) (Fig 8). Thus, the formation of Os rich laurite and erlichmanite (OsS_2) requires a higher fS_2 than for Ru-rich laurite. Consequently, the Ru substitution by Os in laurite is promoted by an increase of fS_2 (Stockman and Hlava, 1984; Brenan and Andrews, 2001). Hence, the common abundance of Os-poor (= Ru-rich) laurite and the later presence of other Os–Ir sulfides and/or alloys in KLIC chromitites suggest that the initial fS_2 of the magma was too low for the formation of Os-rich laurite initially. It is, therefore, highly possible, that the magma involved in the formation of KLIC chromitites was S-undersaturated, and high-temperature boninitic melt with low fS_2 is thus, the most suitable candidate for the formation of PGM in KLIC chromitites (Fig 6).

Several studies explain the inclusions of laurite(RuS_2) grains in Chromites are the most common PGE-bearing phases both in the ophiolitic and layered intrusion chromitites (e.g., Mondal and Baidya, 1997; Mondal, 2000; Mondal et al., 2001; Ahmed, 2007; Habtoor et al., 2017; Mondal et al., 2019). Nevertheless, IPGE-alloys inclusions in Chromites are most typical in ophiolitic Chromites and rare in the mafic-layered intrusions (e.g., Prichard et al., 2017b). All the IPGE alloys in the chromitites of the KLIC are Ru-rich and Os-poor like layered complexes. They also have similarities with the Ru-Os-Ir alloys, which are common

in terrestrial mantle rocks (e.g., Fonseca et al., 2012), whereas alloys from the Ophiolite complexes are Os-rich and Ru-poor and in Alaskan-type complexes are Pt-rich.

5.4. *Role of crustal contamination and it's constrained on Ni-Cu-PGE mineralization*

The consensus is that metal-rich, mantle-derived magmas rarely undergo sulfide saturation and immiscible sulfide melt segregation without undergoing a process of crustal contamination (Keays and Lightfoot, 2010). The role of crustal contamination and assimilation can be easily understand by significant variation in Chromite-PGE composition, which leads to the deposition of Ni-Cu-PGE mineralization (Vuorelainen et al., 1982; Marchetto, 1990; Gervilla and Kojonen, 2002; De Almeida et al. 2007; Naldrett et al., 2008; Piña et al., 2008, 2012; Economou-Eliopoulos, 2010; Kapsiotis et al., 2010; Mondal, 2011; Song et al., 2011; Page et al., 2012; Prichard et al., 2013; Page and Barnes, 2016, O'Driscoll and González-Jimenez, 2016, Evans, 2017; Zaccarini et al., 2018; Mondal et al., 2019; Lu et al., 2019).

Leelanandam and Vijaya Kumar (2007) have mentioned the possibility of the contamination of the magma by pelitic material in the KLIC. Their result suggests that the ultramafic cumulates and constituent minerals has Al_2O_3 enrichment with increasing differentiation, suggesting that the high-Mg parental liquid has delivered, upon differentiation of a high-Al residual magma. They have an opinion that the dominance of orthopyroxene in the chromitite-ultramafic rock series is partly, but not particularly, attested to crustal contamination. The Chromite composition during the present study has indicated minimal crustal contamination as evidence of crystallization of Chromite from a strongly oxidizing magma observed in the TiO_2 vs. Fe^{3+}# diagram (Fig. 3f). Moreover, the limited range of Mg#, Fe^{3+}#, melt TiO_2, Al_2O_3 and (FeO/MgO) supported the insignificant role of massive sedimentary sulfide assimilation, which preclude to the formation of a much larger volume of sulfide melt (high R factor) (Maier et al., 2009; Evans, 2017). Furthermore, Chromite chemistry suggests the S-undersaturated nature of primary magma source, this result also consistent with the presence of primary Ru-rich (and Os–Ir poor, Ni-free) inclusions of PGM at Chromite core. It is indicating that an initial percolation of sulfur-poor melts for a long period without significant contamination for the genesis of KLIC.

There is a very limited availability of metasedimentary rocks for assimilation during the evolution of KLIC, which is also one of the reasons for the insignificant role of crustal contamination and sulfur saturation. As a result, there is no development of potential sulfide mineralization in the KLIC, which is likely to be a product of sulfur-rich melt generated after the significant crustal contamination or assimilations, as reported in many Ni-Cu-PGE

magmatic systems (Song et al., 2011). The KLIC indicated its S-undersaturated magmatic nature, which has limited potential to form Ni-Cu-PGE sulfide deposits, other than S-saturated magmas of fertile melt source. The Ni, Cu, and PGE are strongly partitioning into the sulfide liquids, which leads to the sulfide saturation (S-saturation) and strips metal from the melt to form sulfide deposits. As a result, it produces a chalcophile metal depleted magma. Magmas must, therefore, be S-undersaturated at the time of magma generation and during transport to high crustal levels if they are to form economic concentrations of Ni-Cu-PGE in the crust (Keays, 1995, 1997; Vogel and Keays, 1997).

Several studies suggested that the layered intrusions can be sub-divided into the product of open or closed system magma chambers with a significant role in PGE concentration (Naldrett, 2004; Mungall and Naldrett, 2008). The studies in the past decade also indicated that the intrusions hosting large and super-large magmatic sulfide deposits occur in magma conduits, which provide an open magma system as a perfect environment for the extensive concentration of immiscible sulfide melts, which have been found to occur along deep regional faults (Song et al., 2011). Less commonly, closed-system layered mafic-ultramafic intrusions (LMI) may also contain significant PGE enrichment (e.g., the Platinova Reef of the Skaergaard Intrusion, Greenland). In contrast, the open system magma chamber is contain the most economically significant PGE concentration, predominantly preserved within cumulate sequences in the LMI, which including the development of stratiform chromitite deposits (.g.chromitites occur in the Bushveld Complex and the Stillwater Complex, Montana, USA) (Naldrett, 2004; Mungall and Naldrett, 2008). In such cases, the PGE are frequently, but not ubiquitously associated with these chromitite seams. It maybe results of protracted and high degrees of partial melting that the silicate-hosted sulfides get dissolved in the silicate melt, providing a mechanism by which materials enriched in the IPGE (i.e., Os, Ir, and Ru) can be included in mantle melting (Harvey et al., 2011). Which fever the primary deposition of PGM during the crystallization of Chromite at high temperature in the KLIC.

The present study and previous observations (Meshram et al., 2014, 2015) suggest that the enrichments of the PGE were not significant in the Chromitite-Ultramafic Rock Series within KLIC (i.e., 63–576 ppb ∑PGE), as compared to the major chromitite-hosted PGE deposits. These are suggesting that chromitite PGE abundances can be quite variable in the KLIC.

6. Conclusion:

The present study with the support of texture and compositional variation of Chromite and PGM emphasizes on the genesis of PGE bearing Chromite with tracking subtle changes in the magmatic condition during the evolution of KLIC. The Chromite crystallization initiated by S-undersaturated boninitic melt with the formation of PGM inclusions at higher temperature refers to primary PGM, i.e., Ru-rich laurite and irarsite. The IPGEs probably were fractionated by laurite and irarsite as these minerals are the most common PGMs found in the KLIC chromitites. An alteration changes occur in the composition of laurite, and irarsite are consistent with variation occurs in Chromite from the core to rim, which suggested a complex evolutionary path in the P–T–fS_2–fO_2 space. This also implies that the primary PGM at Chromite core is formed during low fS_2 and high temperature, whereas PGM within altered rim is deposited during high fS_2 and low temperature. As a result, the PGM assemblage reflects considerable mineralogical reworking.

Only Ru-rich laurite and irarsite located in the core of Chromite grains could escape alteration, and possibly represent early magmatic phases. The PGM in the Chromite rim and/or matrix are not consistent with a magmatic origin, i.e., remobilized PGMs. More likely, they represent the product of metamorphism/hydrothermal reworking and remobilization of magmatic PGM. It suggests that PGM integrated the initial magmatic to subsequent secondary imprints during the evolution of KLIC.

The mineral chemistry also supports the minimal crustal contamination and non-availability of the sufficient meta-sediments during assimilation precludes the sulfur saturation in the KLIC, which is mainly constrained for the development of potential Ni-Cu-PGE mineralization. As a result, the KLIC fever the deposition of only primary orthomagmatic Chromite-PGE mineralization form in a magmatic arc setting. In addition, the relevance of fully understanding the textural and compositional diversity and distribution of PGM present in Chromite should not be underestimated during the further exploration work to be carried out in the KLIC. This study can apply to the areas that have similar geochemical characteristics and geodynamic setting.

Acknowledgments:

The Addl. Director General, and The Director, Publication Division, GSI, SR, Hyderabad are thankfully acknowledged for providing their support, encouragement, and approval for this work. The author also acknowledged Smt. Sonalika Joshi (GSI-Hyderabad) for providing the EPMA analysis. Shri. S N Mahapatro is profusely thanked for the valuable suggestions and helpful discussions during different stages of this work. The author expresses

his sincere thanks to Shoji Arai (Kanazawa University, Japan), Federica Zaccarini, Leoben, and Shri Jayant Kumar Nanda for their suggestions and comments during various stages. The author is thankful to two anonymous reviewers for their critical review and constructive comments, which help greatly to improve the manuscript. Finally, the author thanks to Prof. Huayong Chen, Editor-In-Chief and Prof. Alok Porwal, Associate Editor, Ore Geology Reviews for his kind support, encouragement, and consideration of this manuscript for the OGR.

References:

Ahmed, A.H., Arai, S., 2003. Platinum-Group Minerals in podiform chromitites of the Oman ophiolite. The Canadian Mineralogist, 41, 597-616.

Ahmed, A.H., Hanghøj, K., Kelemen, P.B., Hart, S.R., Arai, S., 2006. Osmium isotope systematics of the Proterozoic and Phanerozoic ophiolitic chromitites: in situ ion probe analysis of primary Os-rich PGM. Earth Planet Sci Lett, 245, 777–791.

Aiglsperger, T.,Proenza, J.A.,Zaccarini, F., Lewis, J.F.,Garuti, G., Labrador, M., Longo, F., 2015. Platinum group minerals (PGM) in the Falcondo Ni-laterite deposit, Loma Caribe peridotite Dominican Republic). Mineral. Depos., 50, 105–123.

Arguin, J.P., Page, P., Barnes, S.J., Yu, S.Y., Song, X.Y., 2016. The Effect of Chromite Crystallization on the Distribution of Osmium, Iridium, Ruthenium, and Rhodium in Picritic Magmas: an Example from the Emeishan Large Igneous Province, Southwestern China. Journal of Petrology, 57(5), 1019–1048.

Augé, T., Johan, Z., 1988. Comparative Study of Chromite Deposits from Troodos, Vourinos, North Oman, and New Caledonia Ophiolites. Springer Berlin Heidelberg, 267-288.

Auge, T., Salpeteur, I., Bailly, L., Mukherjee, M.M., Patra, R.N., 2002. Magmatic and hydrothermal platinum-group minerals and base-metal sulfides in the Baula complex, India. The Canadian Mineralogist, 40, 277-309.

Ballhaus, C., Ryan, C.G., 1995. Platinum-group elements in the Merensky Reef. I. PGE in solid solution in base metal sulfides and the down temperature equilibration history of Merensky ores. Contrib Mineral Petr, 122, 241–251.

Barnes, S.J., 2000. Chromite in komatiites, II. Modification during greenschist to mid-amphibolite facies metamorphism. Jour. Petrol. 41, 387-409.

Barnes, S.J., Roeder, P.L., 2001. The range of spinel compositions in terrestrial mafic and ultramafic rocks. Joul. Petrol, 42, 2279–2302.

Barnes, S.J., Ripley, E.M., 2016. Highly siderophile and strongly chalcophile elements in magmatic ore deposits. Rev Mineral Geochem, 81, 725–774.

Brenan, J.M., Andrews, D., 2001. High-temperature stability of laurite and Ru–Os–Ir alloy and their role in PGE fractionation in mafic magmas. Can. Mineral, 39, 341–360.

Bowles, J.F.W., 1986.The development of platinum-group minerals in laterite. Econ. Geol., 81, 1278–1285.

Bowles, J.F.W., Gize, A.P., Vaughan, D.J., Norris, S.J., 1994. Development of platinum group minerals in laterites–initial comparison of organic and inorganic controls. Trans. Ins. Min. Met.(Sec.B,Appl.EarthScs.)103, 53–56.

Chakravarti, S., Mukherjee, S., 1971. Geology and mineralogy of the Chromite deposits occurring near Kondapalle, Krishna district, AP. Jour. Geol. Soc. India, 12, 383-387.

Chaumba, J.B., 2018. Hydrothermal Alteration in the Main Sulfide Zone at Unki Mine, Shurugwi Subchamber of the Great Dyke, Zimbabwe: Evidence from Petrography and Silicates Mineral Chemistry. Minerals, 7(127), 1-43.

Choi, S.H., Shervais, J.W., Mukasa, S.B., 2008. Supra-subduction and abyssal mantle peridotites of the Coast Range ophiolite, California. Contrib. Mineral Petrol, 156, 551–576.

Day, J.M.D., Pearson, D.G., Hulbert, L.J., 2008. Rhenium–osmium isotope and platinum group element constraints on the origin and evolution of the 1.27 Ga Muskox layered intrusion. Jour. Petrol, 49, 1255–1295.

De Almeida, C.M., Olivo, G.R., De Carvalho, S.G., 2007. The Ni–Cu–PGE sulfide ores of the komatiite-hosted Fortaleza De Minas deposit, Brazil: Evidence of hydrothermal remobilization. Can Mineral, 45, 751–773.

Dharma Rao, C.V., Kumar, T.V., Rao, Y.J.B., 2004. The Pangidi Anorthosite Complex, Eastern Ghats Granulite Belt, India: Mesoproterozoic Sm-Nd isochron age and evidence for significant crustal contamination. Curr. Sci., 87(11), 1614-1618.

Dharma Rao, C.V., Santosh, M., 2011. Continental arc magmatism in a Mesoproterozoic convergent margin: Petrological and geochemical constraints from the magmatic suite of Kondapalle along the eastern margin of the Indian plate. Tectonophysics, 510, 151–171.

Dharma Rao, C.V., Santosh, M., Dong, Y., 2011. U–Pb zircon chronology of the Pangidi–Kondapalle layered intrusion, Eastern Ghats belt, India: Constraints on

Mesoproterozoic arc magmatism in a convergent margin setting. Jour. of Asian Earth Sciences, 49, 362–375

Djon, M.L.N., Barnes, S.J., 2012. Changes in sulfides and platinum-group minerals with the degree of alteration in the Roby, Twilight, and High-Grade Zones of the Lac des Iles Complex, Ontario, Canada. Miner Deposita, 47, 875–896.

Dobmeier, C., Raith, M.M., 2003. Crustal architecture and evolution of the Eastern Ghats Belt and adjacent regions of India. In: Proterozoic East Gondwana: Supercontinent Assembly and Breakup. M. Yoshida, B.F. Windley, and S. Dasgupta, (eds). Spl. Pub. Geol. Soc., London, 206, 145-168.

Economou-Eliopoulos, M., 2010. Platinum-group elements (PGE) in various geotectonic settings: Opportunities and risks. Hellenic Journal of Geosciences, 45, 65-82.

Evans, B.W., Frost, B.R., 1975. Chrome-spinel in progressive metamorphism a preliminary analysis. Geochim. Cosmochim. Acta, 39, 959–972.

Evans, D.M., 2015. Metamorphic modifications of the Muremera mafic–ultramafic intrusions, eastern Burundi, and their effect on Chromite compositions. Jour. of African Earth Sciences, 101, 19–34.

Evans, D.M., 2017. Chromite compositions in nickel sulfide mineralized intrusions of the Kabanga-Musongati-Kapalagulu Alignment, East Africa: petrologic and exploration significance. Ore Geology Reviews, 90, 307-321.

Fonseca, R.O.C., Laurenz, V., Mallmann, G., Luguet, A., Hoehne, N., Jochum, K.P., 2012. New constraints on the genesis and long-term stability of Os-rich alloys in the Earth's mantle. Geochim. Cosmochim. Acta, 87, 227–242.

Garuti, G., Zaccarini, F., 1997. In-situ alteration of platinum-group minerals at low temperature: Evidence from chromitites of the Vourinos complex, Greece. Can. Mineral., 35, 611–626.

Garuti, G., Economou-Eliopoulos, M., Zaccarini, F., 1999a. Paragenesis and composition of laurite from the chromitites of Othrys (Greece): implications for Os-Ru fractionation in the upper mantle of the Balkan peninsula. Mineralium Deposita, 34, 312-319.

Garuti, G., Zaccarini, F., Moloshag, V., Alimov, V., 1999b. Platinum-group elements as indicators of sulfur fugacity in the ophiolitic upper mantle: an example from chromitites of the Ray-Iz ultramafic complex, Polar Urals, Russia. Can Mineral, 37, 1099–1115.

Garuti, G., Proenza, J.A., Zaccarini, F., 2007.Distribution and mineralogy of platinum-group elements in altered chromitites of the Campo Formoso layered intrusion (Bahia State, Brazil): Control by magmatic and hydrothermal processes. Mineral. Petrol., 89, 159–188.

Garuti, G., Zaccarini, F., Proenza, J.A., Thalhammer, O.A.R., Angeli, N., 2012. Platinum-group minerals in chromitites of the Niquelândia layered intrusion (Central Goias, Brazil): Their magmatic origin and low-temperature reworking under serpentinization and lateritic weathering. Minerals. 2, 365–384.

Gervilla, F., Kojonen, K., 2002. The platinum-group minerals in the upper section of the Keivitsansarvi Ni–Cu– PGE deposit, northern Finland. Can Mineral, 40, 377–394.

González-Jiménez, J.M., Gervilla, F., Proenza, J.A., Kerestedjian, T., Auge, T., Bailly, L., 2009. Zoning of laurite (RuS_2)–erlichmanite (OsS_2): implications for the origin of PGM in ophiolite chromitites. Eur. Jour. Mineral. 21, 419–432.

Habtoor, M.A., Ahmed, A.H., Akizawa, N., Harbi, H., Arai, S., 2017. Chemical homogeneity of high-Cr chromitites as an indicator for the widespread invasion of boninitic melt in mantle peridotite of Bir Tuluha ophiolite, Northern Arabian Shield. Saudi Arabia. Ore Geol. Rev. 90, 243–259.

Hanley, J.J., 2005. The Aqueous Geochemistry of the Platinum-Group Elements PGE) in Surficial, Low-T Hydrothermal, and High-T Magmatic Hydrothermal Environments. *In:* Exploration for Platinum-Group Element Deposits; Mungall JE (ed) Mineral Assoc Canada: Quebec, QC, Canada. 35–56.

Harvey, J., Dale, C.W., Gannoun, A., Burton, K.W., 2011. Osmium mass balance in peridotite and the effects of mantle-derived sulfides on basalt petrogenesis. Geochim Cosmochim Acta, 75, 5574–5596.

Holwell, D.A., Adeyemi, Z., Ward, L.A., Smith, D.J., Graham, S.D., McDonald, I., Smith, J.W., 2017. Low-temperature alteration of magmatic Ni-Cu-PGE sulfides as a source for hydrothermal Ni and PGE ores: A quantitative approach using automated mineralogy, Ore Geology Rev., 91, 718–740.

Hudson, D.R., Donaldson, M.J., 1984. Mineralogy of platinum group elements in the Kambalda nickel deposits, Western Australia. *In:* Sulphide Deposits in Mafic and Ultramafic Rocks. Buchanan DL, Jones MJ (eds) The Inst Min Metall, 55–61.

Irvine, T.N., 1977. Origin of chromian spinel layers in the Muskoka intrusion and other intrusions: a new interpretation. Geology 5, 273-277.

Ishwar-Kumar, C., Rajesh, V.J., Windley, B.F., Razakamanana, T., Itaya, T., Babu, E.V.S.S.K., Sajeev, K., 2016a. Petrogenesis and tectonic setting of the Bondla ultramafic-mafic complex, western India: Inferences from chromian spinel chemistry. Jour. of Asian Earth Sciences, 130, 192-205.

Ishwar-Kumar, C., Rajesh, V.J., Windley, B.F., Razakamanana, T., Itaya, T., Babu, E.V.S.S.K., Sajeev, K., 2016b. Chromite chemistry as an indicator of petrogenesis and tectonic setting of the Ranomena ultramafic complex in north-eastern Madagascar. Geol. Mag. 155, 109-118.

Kamenetsky, V.S., Crawford, A.J., Meffre, S., 2001. Factors controlling the chemistry of magmatic spinel: an empirical study of associated olivine, Cr-spinel, and melt inclusions from primitive rocks. Jour. Petrol., 42, 655–671.

Kapsiotis, A., Grammatikopoulos, T., Tsikouras, V., Hatzipanagiotou., Zaccarini, F., Garuti, G., 2009. Chromian spinel composition and Platinum group element mineralogy of chromitites from the area of Milia, Pindos ophiolite complex, Greece. Can Mineralogist, 47, 883-902.

Kapsiotis, A., Grammatikopoulos, T.A., Tsikouras, B., Hatzipanagiotou, K., 2010. Platinum-Group Mineral Characterization in Concentrates from High-Grade PGE Al-rich Chromitites of Korydallos Area in the Pindos Ophiolite Complex (NW Greece). Resource Geology, 60(2), 178–191.

Keays, R.R., 1995. The role of komatiitic and picritic magmatism and S-saturation in the formation of ore deposits. Lithos, 34, 1-18.

Keays, R. R., 1997. Requirements for the formation of giant Ni–Cu–PGE sulfide deposits: the role of magma generation. Transactions of the American Geophysical Union EOS, 78, F799.

Keays, R. R. Lightfoot, P. C., 2010. Crustal sulfur is required to form magmatic Ni-Cu sulfide deposits, evidence from chalcophile element signatures of Siberian and Deccan Trap basalts. Mineralium Deposita, 45, 241-257.

Kovach, V.P., Simmat, R., Rickers, K., Berezhnaya, N.G., Salnikova, E.B., Dobmeier, C., Raith, M.M., Yakovleva, S.Z. Kotov, A.B., 2001. The Western Charnockite Zone of the Eastern Ghats Belt, India: an independent crustal province of late Archean (2.8 Ga) and Pelaeoproterozoic (1.7-1.6 Ga) terrains. Gondwana Res., 4, 666-667.

Krishna Rao, J.S.R., 1964. Chromite from Kondapalle, Krishna district, Andhra Pradesh. Jour. Economic Geol, 59, 678-683.

Krupanidhi, K.V.J.R. Subrahmanyam, P., 1969. Geology and Chromite occurrences in the Kondapalli hills of the Krishna district and the Adjoining area of Khammam district, AP. Report Geol. Surv. India

Leelanandam, C., 1967. Report on the Occurrence of anorthosites within the Charnockites of the Kondapalli, AP. Bulletin Geol. Soc. Ind, 4(1), 5-8.

Leelanandam, C., Vijay Kumar, K., 2007. Petrogenesis and Tectonic setting of chromitites and Chromite bearing ultramafic cumulates of the Kondapalli Layered Complex, Eastern Ghat Belt, India: Evidence from the textural, mineral-chemical and whole-rock geochemical studies. Mem. International Assoc. Gond. Res., 10, 89-107.

Leelanandam, C., 1972. An anorthositic layered complex near Kondapalli, Andhra Pradesh. Quart. J. Geol. Mining Metal. Soc. India, 44, 105-107.

Leelanandam, C., 1997. The Kondapalli layered Complex, Andhra Pradesh, India: a synoptic overview. Gondwana Res, 1, 95-114.

Leelanandam, C., 1999. A petrographic and chemical appraisal, and regressive intrusive sequence in the Kondapalli layered Complex, Andhra Pradesh, India. Indian J. Geol, 71, 5-13.

Leelanandam, C., 2006. Dunites, harzburgites, and pyroxenites from Kondapalli: mail from the mantle? Abstract, Group Discussion on The Evolution of the Indian Continental Crust and Upper Mantle: Recent Advances and Future Thrust, Osmania Univ., Hyderabad

Lesher, C.M., Keays, R.R., 2002. Komatiite-associated Ni–Cu–PGE deposits: geology, mineralogy, geochemistry, and genesis. *In:* The Geology, Geochemistry, Mineralogy and Mineral Beneficiation of Platinum-Group Elements. Cabri LJ (ed) Geol Soc CIM, Can Inst Min Metall Petrol Spec Vol, 54, 579–617.

Lu, Y, Lesher, C.M., Deng, J., 2019. Geochemistry and genesis of magmatic Ni-Cu-(PGE) and PGE-(Cu)-(Ni) deposits in China. Ore Geology Rev., 107, 863–887.

Lindsley, D. H., 1983. Pyroxene thermometry. American Mineralogist 68, 477–93.

Lorand, J. P., Luguet, A., 2016.Chalcophile and siderophile elements in mantle rocks: Trace elements controlled by trace minerals. Reviews in Mineralogy and Geochemistry, 81, 441-488.

Maier, W.D., Barnes, S.J., Campbell, I.H., Fiorentini, M.L., Peltonen, P., Barnes, S.J., Smithies, R.H., 2009. Progressive mixing of meteoritic veneer into the early Earth's deep mantle. Nature, 460, 620–623.

Malitch, K.N., Junk, S.A., Thalhammer, O.A.R., Knauf, V.V., Pernika, E. Stumpfl, E.F., 2003. Laurite and ruarsite from podiform chromitites at Kraubath and Hochgrossen, Austria: New insights from osmium isotopes. The Canadian Mineralogist, 41, 331-352.

Marchesi, C., González-Jiménez, J.M., Gervilla, F., Garrido, C.J., Griffin, W.L., O'Reilly, S.Y., Proenza, J.A., Pearson, N.J., 2011. In situ Re-Os isotopic analysis of platinum-group minerals from the Mayarí–Cristal ophiolitic massif (Mayarí–Baracoa Ophiolitic Belt, eastern Cuba): implications for the origin of Os-isotope heterogeneities in podiform chromitites. Contrib Mineral Petrol, 161, 977-990.

Marchetto, C.M.L., 1990. Platinum-group minerals in the O'Toole (Ni–Cu–Co) deposit, Brazil. Econ Geol, 85, 921–927.

Maurel, C., Maurel, P., 1982. Étude experimental de la distribution de l'aluminium entre bain silicate basique et spinel chromifère. Implications pétrogenetiques: tenore en chrome des spinelles. Bulletin de Minéralogie 105, 197–202.

Meshram, T., Nannaware, S.B., Bhattacharjee, S., Rajakumar, T., 2014. Nature of PGE mineralization in the ultramafics of Kondapalli Layered Complex, Andhra Pradesh. Indian Journal of Geosciences, 68(2 & 3), 211-222.

Meshram, T., Nannaware, S.B., Bhattacharjee, S., Waghamare, M., Rajakumar, T., 2015. PGE distribution in the Chromite bearing mafic-ultramafic Kondapalli Layered Complex, Krishna district, Andhra Pradesh, India. Open Geosci., 7, 252-263.

Mezger, K., Cosca, M.A., 1999. The thermal history of the Eastern Ghats Belt (India) as revealed by U-Pb and $^{40}Ar/^{39}Ar$ dating of metamorphic and magmatic minerals: implications for the SWEAT correlation. Precambrian Res., 94, 251-271.

Mondal, S.K., Baidya, T.K., 1997. Platinum group mineral from the Nuasahi ultramafic mafic complex, Orissa. India. Min.Mag., 61, 902–906.

Mondal, S.K., 2000. Study of Chromite, sulfide, and noble metal mineralization in the Precambrian Nuasahi ultramafic-mafic complex, Keonjhar district, Orissa, India. Unpublished Ph.D. thesis. Jadavpur University, Calcutta, India, pp.193.

Mondal, S.K., Baidya, T.K., Rao, K.N.G., Glascock, M.D., 2001. PGE and Ag mineralization in the Breccia zone of the Precambrian Nuasahi ultramafic-mafic complex, Orissa India. Can. Mineral. 39, 979–996.

Mondal, S.K., 2011. Platinum Group Element (PGE) Geochemistry to understand the chemical evolution of the Earth's mantle. Jour. Geol. Soc. of India, 77, 295-302.

Mondal, S. K., Khatun, S., Prichard, H. M., Satyanarayanan, M., Ravindra Kumar, G.R., 2019. Platinum-group element geochemistry of boninite derived Mesoarchean chromitites and ultramafic-mafic cumulate rocks from the Sukinda Massif, Orissa, India, Ore geology Rev., 104, 722-744.

Morimoto, N., 1989. Nomenclature of pyroxenes. Can Mineral, 27, 143–156.

Mukherjee, R., Mondal, S.K., Frei, R., Rosing, M.T., Waight, T.E., Zhong, H., Kumar, G.R.R., 2012. The 3.1Ga Nuggihalli Chromite deposits, Western Dharwar Craton (India): geochemical and isotopic constraints on mantle sources, crustal evolution, and implications for supercontinent formation and ore mineralization. Lithos, 155, 392–409.

Mungall, J.E., Naldrett, A.J., 2008. Ore deposits of the platinum-group elements. Elements, 4, 253–258.

Mungall, J.E., 2014. Geochemistry of magmatic ore deposits. In: Holland, H.D., Turekian, K.K.(eds.), Treatise on Geochemistry, 2nd ed. Elsevier, Oxford, pp.195–218.

Naldrett, A.J., 2004. Magmatic Sulfide Deposits: Geology, Geochemistry, and Exploration. Springer, Berlin

Naldrett, T., Kinnaird, J., Wilson, A., Chunnett, G., 2008. The Concentration of PGE in the Earth's crust with special reference to the Bushveld Complex. Earth Science Frontiers (China University of Geosciences, Beijing; Peking University), 15(5), 264-297.

Naldrett, A.J., 2010. Secular variation of magmatic sulfide deposits and their source magmas. Econ. Geol. 105, 669–688.

Nanda, J. K. Natarajan, V., 1980. Anorthosites and related rocks of the Kondapalli Hills, Andhra Pradesh. Rec. Geol. Surv. India, 113, 57-67.

O'Driscoll, B., Day, J.M.D., Daly, J.S., Walker, R.J., McDonough, W.F., 2009. Rhenium–osmium isotope and platinum-group elements in the Rum Layered Suite, Scotland: Implications for Cr-spinel seam formation and the composition of the Iceland mantle anomaly. Earth Planet Sci Lett, 286, 41–51.

O'Driscoll, B., González-Jimenez, J.M.G., 2016. Petrogenesis of the Platinum-Group Minerals. Reviews in Mineralogy & Geochemistry, Mineralogical Society of America, 81, 489-578.

Oh, C. W., Seo, J., Choi, S. G., Rajesh, V. J. Lee, J. H., 2012. U-Pb SHRIMP zircon geochronology, petrogenesis, and tectonic setting of the Neoproterozoic Baekdong ultramafic rocks in the Hongseong Collision belt, South Korea. Lithos 128–131, 100– 12.

Page, P., Barnes, S.J., Bédard, J.H., Zientek, M.L., 2012. In situ determination of Os, Ir, and Ru in Chromites formed from komatiite, tholeiite, and boninite magmas: Implications for Chromite control of Os, Ir, and Ru during partial melting and crystal fractionation, Chemical Geology, 302–303, 3–15.

Page, P., Barnes, S.J., 2016. The influence of Chromite on osmium, iridium, ruthenium, and rhodium distribution during early magmatic processes. Chemical Geology, 420, 51-68.

Pearce, J.A., Lippard, S.J., Roberts, S., 1984. Characteristics and tectonic significance of supra-subduction zone ophiolites. In: Kokelaar B.P. & Howells M.F. (eds.). Marginal basin geology: volcanic and associated sedimentary and tectonic processes in modern and ancient marginal basins. London, Geological Society of London, Special Publications, 16, 77-94.

Pearson, N.J., Alard, O., Griffin, W.L., Jackson, S.E., O'Reilly, S.Y., 2002. In situ measurement of Re-Os isotopes in mantle sulfides by Laser Ablation Multi-Collector Inductively- Coupled Mass Spectrometry: analytical methods and preliminary results. Geochim Cosmochim Acta, 66, 1037-1050.

Peck, D.C., Huminicki, M.A.E., 2016. Value of mineral deposits associated with mafic and ultramafic magmatism: Implication for exploration strategies. Ore Geology Rev., 72, 269-298.

Piña, R., Gervilla, F., Ortega, L., Lunar, R., 2008. Mineralogy and geochemistry of platinum-group elements in the Aguablanca Ni–Cu deposit (SW Spain). Miner Petrol, 92, 259–282.

Piña, R., Gervilla, F., Barnes, S.J., Ortega, L., Lunar, R., 2012. Distribution of platinum-group and chalcophile elements in the Aguablanca Ni–Cu sulfide deposit (SW Spain): Evidence from an LA-ICP-MS study. Chem Geol, 302–303, 61–75.

Prichard, H.M., Knight, R.D., Fisher, P.C., McDonald, I., Zhou, M.F., Wang, C.Y., 2013. Distribution of platinum-group elements in magmatic and altered ores in the

Jinchuan intrusion, China: an example of selenium remobilization by postmagmatic fluids. Miner Deposita, 48, 767–786.

Prichard, H.M., Mondal, S.K., Mukherjee, R., Fisher, P.C., Giles, N., 2017a. Geochemistry and mineralogy of Pd in the magnetite layer within the upper gabbro of the Mesoarchean Nuasahi Massif (Orissa, India). Miner.Deposita, 53, 547–564.

Prichard, H.M., Barnes, S.-J., Fisher, P.C., Paǵe, P., Zientek, M.L., 2017b. Laurite and associated PGM in the Still water chromitites: implications for processes of formation, and comparisons with laurite in the Bushveld and ophiolitic chromitites. Can. Mineral, 55, 121–144.

Proenza, J.A., Zaccarini, F., Lewis, J.F., Longo, F., Garuti, G., 2007. Chromian spinel composition and the platinum-group minerals of the PGE-rich Loma Peguerachromitites, Loma Caribe peridotite, Dominican Republic. Can. Mineral, 45, 211–228.

Proenza, J.A., Zaccarini, F., Escayola, M., Cábana, C., Schalamuk, A., Garuti, G., 2008. Composition and textures of Chromite and platinum-group minerals in chromitites of the western ophiolitic belt from Pampeans Ranges of Córdoba, Argentina. Ore Geol. Rev., 33, 32–48.

Purvis, A.C., Nesbitt, R.W., Hallberg, J.A., 1972. The geology of part of the Carr Boyd Rocks complex and its associated nickel mineralization, Western Australia. Economic Geology, 67, 1093-1113.

Roeder, P.L., Campbell, I.H., 1985. The effect of postcumulus reactions on the composition of chrome-spinels from the Jimberlana intrusion. Jour. Petrol, 26(3), 763-786.

Rogers, J.J.W., Santosh, M., 2002. Configuration of Columbia, a Mesoproterozoic supercontinent. Gondwana Res., 5, 5-22.

Rogers, J.J.W. Santosh, M., 2004. Continents and Supercontinents. Oxford Univ. Press, New York, 289.

Rollinson, H., 2008. The geochemistry of mantle chromitite from the northern part of the Oman ophiolite: inferred parental melt compositions. Contr. to Mineral and Petrol., 156, 273–288.

Sack, R.O., Ghiorso, M.S., 1991. Chromian spinels as petrogenetic indicators: thermodynamic and petrological applications. American Mineralogist, 76, 827–847.

Scoates J.S., Friedman, R.M., 2008. The precise age of the platiniferous Merensky Reef, Bushveld Complex, South Africa, by the U–Pb Zircon chemical abrasion ID-TIMS technique. Econ Geol, 103, 465–471.

Seabrook, C.L., Prichard, H.M., Fisher, P.C., 2004. Platinum-group minerals in the Raglan Ni–Cu–(PGE) sulfide deposit, Cape Smith, Quebec, Canada. Can Mineral 42, 485–497.

Shcheka, G.G., Lehmann, B., Gierth, E., Gömann, K., Wallianos, A., 2004. Macrocrystals of Pt–Fe alloy from the Kondyor PGE placer deposit, Khabarovskiy Kray, Russia: trace-element content, mineral inclusions, and reaction assemblages. Can Mineral, 42, 601–617.

Shi, R., Alard, O., Zhi, X., O'Reilly, S.Y., Pearson, N.J., Griffin, W.L., Zhang, M., Chen, X., 2007. Multiple events in the Neo-Tethyan oceanic upper mantle: evidence from Ru–Os–Ir alloys in the Luobusa and Dongqiao ophiolitic podiform chromitites, Tibet. Earth Planet Sci Lett., 261, 33–48.

Slansky, E., Johan, Z., Ohnenstetter, M., Barron, L.M. Suppel, D., 1991. Platinum mineralization in the Alaskan type intrusive complexes near Fifield, N.S.W., Australia. 2. Platinum-group minerals in placer deposits at Fifield. Mineral. Petrol., 43, 161-180.

Song X., Wang, Y., Chen, L., 2011. Magmatic Ni-Cu-(PGE) deposits in magma plumbing systems: Features, formation, and exploration. Geoscience Frontiers, 2(3), 375-384.

Stockman, H.W., Hlava, P.F., 1984. Platinum-group minerals in Alpine chromitites from south-western Oregon. Econ Geol, 79, 491-508.

Suárez, S., Prichard, H.M., Velasco, F., Fisher, P.C., McDonald, I., 2010. Alteration of platinum-group minerals and dispersion of platinum-group elements during progressive weathering of the Aguablanca Ni–Cu deposit, SW Spain. Miner Deposita, 45, 331–350.

Suita, M.T., Streider, A.J., 1996. Cr-spinels from Brazilian mafic-ultramafic complexes: metamorphic modifications. International Geology Rev., 38, 245-267.

Tamura, A., Arai, S., 2006. Harzburgite-dunite orthopyroxenite suite as a record of supra-subduction zone setting for the Oman ophiolite mantle. Lithos, 90, 43–56.

Upadhyay, D., Raith, M.M., Mezger, K., and Hammerschmidt, K., 2006. Mesoproterozoic rift-related alkaline magmatism at Elchuru, Prakasam Alkaline Province, SE India. Lithos, 89, 447-477.

Uysal, I., Zaccarini, F., Garuti, G., Meisel, T., Tarkian, M., Bernhardt, H. J., Sadiklar, M. B., 2007. Ophiolitic chromitites from the Kahramanmaras area, southeastern Turkey: their platinum group elements (PGE) geochemistry, mineralogy, and Os-isotope signature. Ofioliti, 32, 151-161.

Vernon, R.H., 2004. A Practical Guide to Rock Microstructure. Cambridge Univ. Press, pp-594.

Vijaya Kumar, K., Frost, C.D., Frost, B.R., Chamberlain, K.R., 2007. The Chimakurti, Errakonda, and Uppalapadu plutons, Eastern Ghats Belt, India: an unusual association of tholeiitic and alkaline magmatism. Lithos, 97, 30-57.

Vogel, D.C., Keays, R.R., 1997. The petrogenesis and platinum group element geochemistry of the Newer Volcanic Province, Victoria, Australia. Chemical Geology, 136, 181–204.

Vuorelainen, Y., Häkli, T.A., Hänninen, E., Papunen, H., Reino, J., Törnroos, R., 1982. Isomertieite and other platinum-group minerals from the Konttijärvi layered mafic intrusion, northern Finland. Econ Geol, 77, 1511–1518.

Wilson, M., 1989. Igneous Petrogenesis: A Global Tectonic Approach; Unwin Hyman, London, pp-466.

Zaccarini, F., Proenza, J.A., Ortega-Gutierrez, F., Garuti, G., 2005. Platinum-group minerals in ophiolitic chromitites from Tehuitzingo (Acatlan complex, southern Mexico): Implications for postmagmatic modification. Mineral. Petrol. 84, 147–168.

Zaccarini, F., Pushkarev, E., Garuti, G., 2008.Platinum-group element mineralogy and geochemistry of chromitite of the Kluchevskoy ophiolite complex, central Urals (Russia). Ore Geol. Rev. 33, 20–30.

Zaccarini, F., Proenza, J.A., Rudashevsky, N.S., Cabri, L.J., Garuti, G., Rudashevsky, V.N., Melgarejo, J.C., Lewis, J.F., Longo, F., Bakker, R.J., 2009. The Loma Pegueraophioliticchromitite (Central Dominican Republic): A source of new platinum-group minerals (PGM) species. Jour. Mineral. Geochem. 185, 335–349.

Zaccarini, F., Garuti, G., Proenza, J.A., Campos, L., Thalhammer, O.A.R., Aiglsperger, T., Lewis, J., 2011. Chromite and platinum-group-elements mineralization in the Santa Elena ophiolitic ultramafic nappe (Costa Rica): Geodynamic implications. Geol. Acta, 9, 407–423

Zaccarini, F., Idrus, A., Garuti, G., 2016. Chromite Composition and Accessory Minerals in Chromitites from Sulawesi, Indonesia: Their Genetic Significance, Minerals, 6(46), 1-23.

Zaccarini, F., Garuti, G., Pushkarev, E., Thalhammer, O., 2018. Origin of Platinum Group Minerals (PGM) Inclusions in Chromite Deposits of the Urals. Minerals, 8, 379, 1-21.

Zhou, M.F., Robinson, P.T., Malpas, J., Zijin, L., 1996. Podiform Chromites in the Luobusa Ophiolite (Southern Tibet): implications for melt–rock interaction and Chromite segregation in the upper mantle. Jour. Petrol., 37, 3-21.

Description of Figures:

Figure 1: (a) Geological map of Kondapalli area showing the location of dismembered Kondapalli Layered Igneous Complex (Inset map of India shows the location of the study area within EGB). **(b)** Inset map of India showing the location of the Study area within the Eastern Ghat Granulite Belt. **(c)** Locations of the arc-related Kondapalle layered complex and the Chimalpahad anorthosite complex. The Map also shows the location of Sukinda and Nausahi dismembered ophiolites at the sutured margins along the craton-mobile belt (map modified from Dharma Rao and Santosh, 2011).

Figure 2: (a) Field photographs showing rhythmic banding of chromite and pyroxenite layers at the Nakkerlapadu quarry. **(b)** Field photograph showing chromite mineralization and development of serpentine from pyroxenite at Gangineni quarry (GQ, Fig. 1). **(c)** Photomicrographs showing the chromite cumulate with intercumulus pyroxenes (Gangineni quarry, GQ-2, Fig. 1). **(d)** Photomicrographs showing the brown color chromite cumulate with intercumulus pyroxenes, which are altered to serpentine (Gangineni quarry, GQ-1, Fig. 1). **(e)** Backscattered electron image showing the triple junction grain boundary within chromite cumulates (Loyya quarry, LQ, Fig. 1). **(f)** Backscattered electron image showing variation in chromite composition from Cr- rich core to Fe- rich rim (Gangineni quarry, GQ-1, Fig. 1). (Abbreviations, Chr-Chromite, Opx-Orthopyroxene, Ser-Serpentine)

Figure 3: (a) Cr-Al-Fe^{3+} (atomic proportions) diagram for mineral compositions of chromites. Fields are after Barnes and Roeder (2001) and Stevens (1944). **(b)** Orthopyroxene composition from the chromitites of KLIC in an experimentally contoured Ca–Mg–Fe phase-relation diagram at 1.0 GPa (after Lindsley, 1983). **(c)** The binary diagram of Cr_2O_3 vs Al_2O_3

and **(d)** Cr_2O_3 vs FeO shows the variation in chromite composition from the core to rim. **(e)** Mg# vs. Cr# diagram for chromite of KLIC. **(f)** Fe^{3+}# vs. TiO_2 variation diagram show liquid reaction indices of chromite in the KLIC. Dashed lines indicate the 90 percent and 50 percent fields of chrome-spinels in layered intrusions from the compilation by Barnes and Roeder (2001).

Figure 4: (a) Cr# versus Fe^{2+}# for chromite from studied sample plots near the plutonic chromite (layered intrusion stratiform chromite). The degree of partial melting scale is from Pagé et al. (2008) based on batch melting experiments from Hirose and Kawamoto (1995) (The inset shows the two groups of chromite, group 1 has low Fe^{2+}# (<42.5) and group 2 has high Fe^{2+}# (>45.8), see text for more details.) **(b)**Classification of chromite After Barnes and Roeder, 2011, KLIC falls in layered intrusion. **(c)** Fe^{3+}-ratio (Fe^{3+}/(Fe^{3+} + Al + Cr) atomic ratio) versus Mg-ratio (Mg/(Mg+ Fe^{2+}) atomic ratio) variation diagram.

Figure 5: (a) Ternary Cr-Al-Fe^{3+} diagram exhibiting chromite analysis from KLC chromitites, after Proenza, et al. 2008 with the fields of different metamorphic facies from Purvis, et al., 1972; Evans, and Frost 1975; De Freitas Suita and Strieder, 1996. Similarly, compare the Al–Cr–Fe^{3+} ternary diagram for chromite compositions from the Chromitites of KLIC, which plot on the spinel stability boundary (Sack & Ghiorso, 1991), calculated for spinel in equilibrium with Fo_{90} olivine. **(b)** Plots of Cr# vs TiO_2 wt% in chromian spinel after Choi et al. (2008). **(c)** Al_2O_3 (wt%) vs Mg# for pyroxenes (CPX = clinopyroxene; OPX = orthopyroxene). Fields of primary clinopyroxenes in Izu–Bonin–Mariana (IBM) forearc peridotites from Ishii et al. (1992), Parkinson and Pearce (1998); the secondary or retrograde clinopyroxenes from Khedr, Arai, Tamura, and Morishita (2010) and references therein; field for abyssal clinopyroxene and orthopyroxene and SSZ peridotite clinopyroxene from Choi, Shervais, and Mukasa (2008).

Figure 6: (a) Plot of TiO_2 versus Al_2O_3 wt% in chromian spinels. Tectonic discrimination fields are after Kamenetsky et al. (2001). SSZ: Supra-subduction zone; LIP: large igneous province; MORB: mid-ocean ridge basalt; OIB: ocean island basalt. **(b)** Cr/Cr+Al versus TiO_2 diagram for chromian spinels of the KLC. Tectonic fields of fore-arc harzburgites/peridotites from Ishii et al. (1992), Parkinson and Pearce (1998), Pearce et al. (2000), the abyssal peridotites field is from Dick and Bullen (1984), and the boninites field is from van der Laan et al. (1992). **(c)** Tectonic discrimination diagrams for chromite, Cr/(Cr+Al) v. Mg/(Mg+Fe^{2+}) (after Tamura and Arai, 2006; Oh et al., 2012). **(d)** Al_2O_3 in melts v. Al_2O_3 in spinel (after, Rollinson, 2008), based on melt calculations of Maurel and Maurel (1982).

Figure 7: Representative backscattered images of PGM and BMS in the KCL **(a-c-h)** Laurite grain along the border between chromite and opx and also inclusion within chromite. **(b-d)** Irarsite grain occurs as small inclusion within chromite/opx. **(e)** Silver grain occurs as inclusion near the border of chromite. **(f-g)** Pentlandite and millerite occur interstitial to chromite with associated serpentine and relict orthopyroxene (opx).

Figure 8: (a) The ternary OsS_2-RuS_2-IrS_2 diagram shows the variation of PGM present in chromite core and chromite rim**. (b)** The ternary (S+Ni+Fe)-(Rh+Pt+Pd)-(Os+Ru+Ir) diagram to show the nature of PGM and sulfides within KLIC. **(c)** Phase diagram of the Pt+(Fe, Cu) – Os+(Ru) – Ir+(Rh) system (Slansky et al. 1991) (field for Two-phase paragenesis taken from Shcheka & Vrzhosek, 2004).

Figure 9: The binary variation diagram of Ru vs Ir, Os, Rh, Pt, Pd, S and As showing trends from PGM situated in chromite core and rim.

Table.1a: Representative EPMA analysis of chromite core from the KLC.

Table.1a: Representative EPMA analysis of chromite rim from the KLC.

Table.2: Representative EPMA analysis of orthopyroxenes from KLC.

Table.3: Representative EPMA analysis of PGM from KLC.

Table No 1a Representative EPMA analysis of chromite core from KLIC

Data Set	*11*	*12*	*13*	*14*	*15*	*17*	*18*	*19*	*23*	*36*	*37*	*38*	*39*	*40*	*41*	*42*	*43*	*44*	*45*	*46*	*47*	*49*	*50*	*52*	*55*	*56*	*61*	*62*	*63*
	BQ	*BQ*	*BQ*	*BQ*	*BQ*	*BQ*	*BQ*	*BQ*	*LQ*	*LQ*	*LQ*	*LQ*	*LQ*	*LQ*	*NQ*	*NQ*	*NQ*	*NQ*	*NQ*	*NQ*	*NQ*	*NQ*	*NQ*	*GQ*	*GQ*	*GQ*	*GQ*	*GQ*	*GQ*
TiO2	0.262	0.201	0.183	0.218	0.197	0.17	0.217	0.184	0.306	0.236	0.217	0.197	0.188	0.246	0.112	0.253	0.246	0.26	0.254	0.249	0.174	0.288	0.222	0.256	0.304	0.285	0.272	0.315	0.324
Al2O3	11.30	11.55	11.39	12.05	11.52	11.74	12.35	11.13	12.83	11.02	11.29	11.36	11.05	10.76	11.11	10.93	10.63	11.26	11.55	11.04	11.62	11.62	10.86	11.91	12.37	12.02	12.40	12.23	12.36
Cr2O3	56.56	55.30	55.57	55.48	54.91	54.96	53.98	56.63	50.54	54.34	54.38	53.86	56.31	56.05	54.74	54.87	54.37	54.39	54.58	55.70	54.81	53.33	55.26	52.21	50.54	51.56	50.54	50.78	51.71
FeO	22	22	22	21	22	22	22	22	28	24	24	25	23	23	24	24	24	24	25	23	23	25	24	28	28	27	28	27	27

T	.25	.89	.29	.86	.40	.13	.20	.60	.41	.73	.02	.33	.51	.67	.17	.88	.45	.66	.04	.66	.41	.62	.00	.02	.46	.91	.18	.74	.99
MnO	0.329	0.332	0.301	0.294	0.224	0.319	0.351	0.359	0.405	0.31	0.305	0.408	0.313	0.267	0.334	0.288	0.351	0.284	0.315	0.371	0.332	0.366	0.324	0.38	0.414	0.425	0.387	0.392	0.399
MgO	9.042	9.552	9.2422	9.3227	9.2955	9.3944	9.2557	8.9886	6.6883	8.362	8.8944	8.8654	8.2116	8.4511	9.003	8.3944	8.3307	8.6266	8.9977	8.6223	8.5225	8.8229	8.3999	6.5669	6.7551	6.6	6.5526	6.5811	6.5996
Total	99.77	99.87	99.05	99.32	98.55	98.80	98.43	99.92	99.26	99.04	99.15	99.83	99.84	99.53	99.65	99.64	98.44	99.41	100.72	99.02	99.41	100.1	99.22	99.47	99.02	99.09	98.35	98.10	99.36
Fe2O3	2.5000	4.2445	3.2334	2.7488	3.4200	3.5226	3.1744	2.9447	5.5119	4.7144	4.6266	5.5033	3.4511	3.4433	5.1588	4.5488	4.4334	4.5611	5.2347	3.5887	3.6066	5.9449	4.3100	5.2331	6.2881	5.8222	5.4766	5.1011	4.7669
FeO	20.00	19.07	19.38	19.38	19.32	18.96	19.34	19.95	23.45	20.49	19.85	20.38	20.41	20.57	19.53	20.78	20.46	20.55	20.33	20.43	20.17	20.27	20.12	23.31	22.81	22.67	23.26	23.15	23.70
Total	100.0	100.2	99.37	99.59	98.90	99.15	98.75	100.2	99.81	99.51	99.62	100.63	100.1	99.88	100.1	100.0	98.88	99.87	101.2	100.0	99.38	100.7	99.66	99.99	99.65	99.67	98.90	98.61	99.84
Ti	0.007	0.005	0.005	0.005	0.005	0.004	0.005	0.005	0.008	0.006	0.005	0.005	0.005	0.006	0.003	0.006	0.006	0.007	0.006	0.006	0.004	0.007	0.006	0.006	0.008	0.007	0.007	0.008	0.008
Al	0.441	0.448	0.447	0.470	0.453	0.460	0.485	0.434	0.507	0.435	0.443	0.443	0.433	0.423	0.434	0.429	0.423	0.442	0.446	0.433	0.457	0.451	0.428	0.472	0.490	0.477	0.496	0.490	0.490
Cr	1.480	1.438	1.461	1.450	1.449	1.444	1.420	1.481	1.340	1.438	1.431	1.410	1.480	1.478	1.432	1.445	1.450	1.432	1.413	1.463	1.445	1.389	1.460	1.387	1.343	1.372	1.355	1.365	1.374
Fe+3	0.062	0.105	0.081	0.068	0.086	0.088	0.080	0.073	0.139	0.119	0.116	0.137	0.086	0.086	0.128	0.114	0.113	0.114	0.129	0.090	0.091	0.147	0.108	0.132	0.159	0.147	0.140	0.130	0.121
Fe+2	0.554	0.525	0.539	0.536	0.539	0.527	0.538	0.552	0.658	0.574	0.553	0.564	0.567	0.574	0.541	0.579	0.577	0.572	0.557	0.568	0.563	0.558	0.562	0.655	0.641	0.638	0.660	0.658	0.666
Mn	0.0	0.0	0.0	0.0	0.0	0.0	0.0	0.0	0.0	0.0	0.0	0.0	0.0	0.0	0.0	0.0	0.0	0.0	0.0	0.0	0.0	0.0	0.0	0.0	0.0	0.0	0.0	0.0	0.0

	09	09	08	08	06	09	10	10	12	09	09	11	09	08	09	08	10	08	09	10	09	10	09	11	12	12	11	11	11
Mg	0.446	0.468	0.458	0.459	0.462	0.465	0.459	0.443	0.334	0.417	0.441	0.427	0.407	0.420	0.444	0.417	0.418	0.428	0.439	0.427	0.424	0.434	0.418	0.329	0.338	0.331	0.330	0.333	0.330
Cr#	77.04	76.24	76.58	75.53	76.17	75.84	74.56	77.33	72.53	76.78	76.36	76.07	77.36	77.74	76.76	77.10	77.42	76.40	76.00	77.18	75.98	75.47	77.33	74.62	73.26	74.19	73.22	73.57	73.72
Mg#	44.62	47.15	45.94	46.16	46.16	46.89	46.03	44.53	33.68	42.10	44.39	43.08	41.77	42.26	45.09	41.85	41.98	42.78	44.09	42.92	42.96	43.70	42.65	33.43	34.52	34.15	33.33	33.62	33.15
Fe3+#	6.556	10.28	8.2111	6.8511	8.5755	8.7022	7.7688	7.7178	14.20	12.23	11.58	13.60	9.3155	9.2966	12.76	11.87	11.80	11.60	12.71	9.4447	9.3220	14.28	11.35	14.17	16.09	15.42	14.47	13.67	12.81
Melt (Al2O3)	9.458	8.54	9.095	8.036	8.8001	8.3611	7.489	9.97	6.384	9.451	8.937	8.586	9.722	9.8811	9.1022	9.6565	9.8881	8.9652	8.2966	9.6565	8.56	7.9972	9.8881	7.719	6.8112	7.41	6.9229	7.2277	7.1077
FeO/MgO	0.652	0.567	0.6143	0.6533	0.6143	0.62	0.6669	0.6333	0.8889	0.6488	0.6122	0.6225	0.677	0.6556	0.5722	0.6511	0.6422	0.6488	0.6113	0.6533	0.6822	0.6144	0.6335	0.8557	0.8399	0.8838	0.8811	0.8777	0.8922

Table No 1b Representative EPMA analysis of chromite altered rim from KLIC

DataSet	***1***	***2***	***3***	***5***	***6***	***7***	***22***	***24***	***25***	***26***	***27***	***29***	***30***	***31***	***32***	***33***	***34***	***35***	***48***	***54***	***57***	***60***	***65***	***70***	***71***	***73***	***74***	***75***	***80***	***82***	***84***
	BQ	***BQ***	***BQ***	***BQ***	***BQ***	***BQ***	***LQ***	***LQ***	***LQ***	***LQ***	***LQ***	***LQ***	***LQ***	***LQ***	***LQ***	***LQ***	***LQ***	***LQ***	***NQ***	***GQ***	***GQ***	***GQ***	***GQ***	***GQ***	***GQ***	***GQ***	***GQ***	***GQ***	***NQ***	***NQ***	***NQ***
TiO2	0.32	0.33	0.36	0.27	0.25	0.32	0.31	0.33	0.32	0.22	0.33	0.24	0.27	0.23	0.27	0.32	0.32	0.30	0.31	0.26	0.28	0.29	0.29	0.29	0.31	0.29	0.33	0.35	0.29	0.36	0.37

Al_2O_3	11.51	10.86	10.56	10.59	11.07	10.72	13.56	12.84	13.27	13.17	13.53	13.32	13.12	13.01	13.32	13.36	13.45	13.38	13.89	12.39	12.86	11.59	12.11	15.58	17.03	16.45	17.02	16.60	14.88	15.49	15.15
Cr_2O_3	44.97	44.42	44.41	44.13	43.67	44.86	49.04	48.42	49.97	49.28	48.61	48.97	47.53	47.65	48.58	48.98	47.10	49.48	48.24	49.19	48.17	49.16	49.77	45.58	45.95	45.68	45.27	42.87	44.74	44.35	45.24
FeOT	36.78	37.38	36.91	38.00	37.62	36.91	28.66	29.59	28.79	29.66	29.73	30.20	30.84	31.17	30.09	29.71	31.13	29.35	28.33	31.10	31.26	30.86	29.97	30.15	27.35	28.80	27.48	31.30	30.92	31.41	30.54
MnO	0.38	0.37	0.40	0.42	0.44	0.38	0.38	0.39	0.40	0.39	0.40	0.42	0.37	0.33	0.38	0.30	0.36	0.30	0.32	0.38	0.36	0.35	0.45	0.35	0.33	0.29	0.25	0.37	0.40	0.31	0.30
MgO	4.51	4.91	4.79	4.82	5.01	5.02	6.54	6.92	6.78	6.70	6.93	6.66	7.00	6.83	6.59	6.91	6.71	6.72	8.03	6.29	6.55	6.14	6.28	6.97	8.25	7.98	8.08	7.86	7.28	7.48	7.42
Total	98.60	98.38	97.38	98.28	98.08	98.27	98.52	98.53	99.64	99.42	99.57	99.85	99.20	99.36	99.21	99.55	99.14	99.58	99.26	99.77	99.66	99.44	99.92	99.29	99.47	99.51	99.40	99.45	99.49	99.40	99.07
Fe_2O_3	11.33	13.01	12.44	13.63	13.47	12.61	5.53	7.40	5.80	6.87	7.00	7.14	8.65	8.68	6.80	6.90	8.20	6.22	7.48	8.17	8.57	7.76	6.86	8.66	6.01	7.11	6.20	10.01	9.10	9.33	8.55
FeO	26.58	25.67	25.71	25.73	25.50	25.56	23.68	22.93	23.58	23.48	23.43	23.78	23.06	23.36	23.97	23.50	23.75	23.75	21.60	23.75	23.56	23.87	23.80	22.35	22.94	22.40	21.90	22.29	22.73	23.01	22.84
Total	99.73	99.68	98.63	99.64	99.43	99.53	99.08	99.27	100.22	100.11	100.27	100.56	100.07	100.23	100.89	100.24	99.96	100.20	100.01	100.58	100.52	99.22	99.60	100.82	99.90	100.18	99.13	100.46	99.40	100.34	99.93
Ti	0.011	0.011	0.011	0.011	0.011	0.011	0.011	0.011	0.011	0.011	0.011	0.011	0.011	0.011	0.011	0.011	0.011	0.011	0.011	0.011	0.011	0.011	0.011	0.011	0.011	0.011	0.011	0.011	0.011	0.011	0.011
Al	0.447	0.443	0.433	0.435	0.444	0.454	0.511	0.522	0.522	0.533	0.522	0.522	0.511	0.533	0.522	0.533	0.533	0.544	0.499	0.511	0.477	0.488	0.600	0.655	0.633	0.666	0.666	0.644	0.588	0.600	0.599
Cr	1.222	1.211	1.220	1.219	1.222	1.231	1.299	1.232	1.330	1.300	1.288	1.299	1.225	1.266	1.299	1.299	1.244	1.300	1.266	1.300	1.277	1.322	1.333	1.177	1.188	1.188	1.177	1.110	1.188	1.155	1.188
Fe^{+3}	0.299	0.344	0.333	0.355	0.355	0.333	0.144	0.199	0.155	0.177	0.188	0.188	0.222	0.222	0.177	0.177	0.211	0.166	0.199	0.211	0.211	0.200	0.177	0.211	0.155	0.177	0.155	0.255	0.233	0.233	0.211
F	0	0	0	0	0	0	0	0	0	0	0	0	0	0	0	0	0	0	0	0	0	0	0	0	0	0	0	0	0	0	0

e+2	.76	.74	.75	.74	.73	.74	.67	.65	.66	.66	.65	.66	.64	.65	.67	.65	.66	.66	.60	.66	.66	.68	.67	.61	.60	.61	.60	.61	.63	.63	.63
Mn	0.01	0.01	0.01	0.01	0.01	0.01	0.01	0.01	0.01	0.01	0.01	0.01	0.01	0.01	0.01	0.01	0.01	0.01	0.01	0.01	0.01	0.01	0.01	0.01	0.01	0.01	0.01	0.01	0.01	0.01	0.01
Mg	0.23	0.25	0.25	0.25	0.26	0.26	0.33	0.35	0.34	0.33	0.34	0.33	0.35	0.34	0.33	0.34	0.33	0.33	0.40	0.31	0.33	0.31	0.32	0.39	0.40	0.39	0.39	0.38	0.36	0.37	0.37
Cr#	72.39	73.30	73.82	73.66	72.57	73.72	70.81	71.68	71.63	71.51	70.67	71.15	70.84	71.06	70.99	71.10	70.14	71.27	69.97	72.70	71.54	73.99	73.38	66.25	64.42	65.07	64.08	63.40	66.86	65.76	66.70
Mg#	23.23	25.43	24.91	25.02	25.94	25.91	33.00	34.96	33.90	33.70	34.51	33.30	35.10	34.24	32.88	34.37	33.50	33.53	39.86	32.06	33.15	31.43	31.98	38.87	40.13	38.83	39.66	38.60	36.33	36.67	36.66
Fe3+#	29.60	32.74	32.34	34.28	33.07	32.05	13.92	17.96	14.48	16.85	16.71	17.33	20.08	20.37	16.71	16.62	19.26	15.37	16.56	20.40	20.55	20.39	17.92	17.72	12.26	14.61	12.69	19.41	19.45	19.28	18.21

Data Set	*10*	*21*	*28*	*4*	*51*	*53*	*58*	*59*	*66*	*76*	*78*	*8*	
SiO2	56.32	56.6	58.38	56.1	56.6	56.39	57.1	56.01	57.61	56.07	57.2	56.21	56
TiO2	0.064	0.129	0.056	0.039	0.028	0.099	0.027	0.074	0.077	0.082	0.055	0.104	0.
Al2O3	1.015	1.464	1.339	1.122	1.239	0.98	0.934	1.279	1.31	1.748	1.485	1.296	1.
FeOt	9.573	7.901	7.645	9.559	7.883	7.333	7.709	7.876	7.359	7.113	7.695	9.442	7.
Cr2O3	0.38	0.586	0.562	0.336	0.559	0.384	0.602	0.393	0.387	0.475	0.355	0.374	0.
MnO	0.224	0.155	0.167	0.221	0.208	0.181	0.104	0.154	0.159	0.118	0.173	0.251	0.
MgO	30.83	31.86	32.91	30.56	31.39	33	32.47	31.73	32.63	32.6	32.58	30.54	32
CaO	0.578	0.312	0.264	0.36	0.359	0.18	0.194	0.402	0.124	0.303	0.226	0.515	0.
Na2O	0.026	0.002	0.037	0	0	0.046	0.05	0.069	0.022	0.029	0.013	0.023	0.
K2O	0.014	0.014	0.015	0.007	0.004	0.023	0	0.027	0.035	0.003	0.018	0.009	0.
Total	99.03	99.02	101.4	98.3	98.27	98.61	99.19	98.02	99.64	98.53	99.76	98.74	98
Ca	1.131	0.613	0.506	0.713	0.713	0.346	0.377	0.791	0.241	0.591	0.437	1.018	0.
Mg	83.91	87.04	87.8	84.17	86.74	88.36	87.77	86.87	88.34	88.41	87.68	84.02	87
Fe2_Mn	14.96	12.35	11.7	15.12	12.55	11.29	11.85	12.34	11.42	11	11.88	14.97	11
Mg#	0.849	0.876	0.882	0.848	0.874	0.887	0.881	0.876	0.886	0.889	0.881	0.849	0.
Q	1.937	1.919	1.915	1.929	1.912	1.953	1.933	1.931	1.918	1.932	1.927	1.922	1.
J	0.004	0	0.005	0	0	0.006	0.007	0.01	0.003	0.004	0.002	0.003	
WO	1.131	0.613	0.506	0.713	0.713	0.346	0.377	0.791	0.241	0.591	0.437	1.018	0.

EN	83.91	87.04	87.8	84.17	86.74	88.36	87.77	86.87	88.34	88.41	87.68	84.02	87
FS	14.96	12.35	11.7	15.12	12.55	11.29	11.85	12.34	11.42	11	11.88	14.97	11

Table No.3. Repre

Data Set	***13***	***14***	***18***	***31***	***32***	***33***	***35***	***36***	***40***	***41***	***46***	***47***	***42***	***4***
	GQ-1	***GQ-1***	***GQ-1***	***GQ-2***	***GQ-2***	***GQ-2***	***GQ-2***	***GQ-2***	***GQ-2***	***GQ-2***	***GQ-2***	***GQ-2***	***GQ-2***	***GQ-2***
Mineral	***Laurite core***	***Laurite core***	***laurite rim***	***laurite rim***	***laurite rim***	***laurite rim***	***laurite rim***	***laurite rim***	***laurite rim***	***laurite rim***	***erlichmentite***	***erlichmentite***	***irarsite core***	
S	32.482	36.173	29.579	30.598	30.613	28.659	29.309	30.729	27.813	28.568	26.622	27.181	12.836	12.07
Fe	0.623	0.67	0.458	2.985	3.092	3.723	2.769	2.867	2.734	2.93	2.97	3.138	2.06	0.5
Ni	0.359	0.377	0.224	0.134	0.171	0.088	0.107	0.064	0.087	0.1	0.112	0.139	0.009	
Cu	0.181	0.041	0.086	0.104	0.023	0	0.015	0.043	0.02	0.039	0.13	0.134	0.46	0.58
Pb	0	0	0	0	0	0	0	0	0	0	0	0	0	
As	0.542	0.668	3.513	0.657	0.597	0.594	0.643	0.654	0.826	0.779	2.644	2.492	25.667	23.08
Pd	2.52	2.517	1.266	1.548	1.536	1.333	1.463	1.643	0.572	0.549	0.461	0.506	0.407	0.40
Ru	50.531	49.049	23.494	30.74	31.985	31.258	30.156	31.508	8.246	8.936	9.044	9.163	0.58	0.42
Rh	2.378	2.34	1.539	1.828	1.879	1.916	1.773	1.975	1.239	1.312	0.57	0.918	2.065	2.07
Pt	0.18	0.268	0.633	0.231	0.104	0.024	0.09	0.105	0.232	0.089	0.357	0.188	2.029	0.1
Os	4.27	4.891	31.948	21.448	21.503	20.754	21.022	21.348	49.917	48.89	42.027	41.425	2.852	1.83
Ir	4.283	4.129	7.96	3.932	3.979	3.929	4.205	3.909	7.111	7.128	15.518	15.213	54.827	57.77

Figure_1

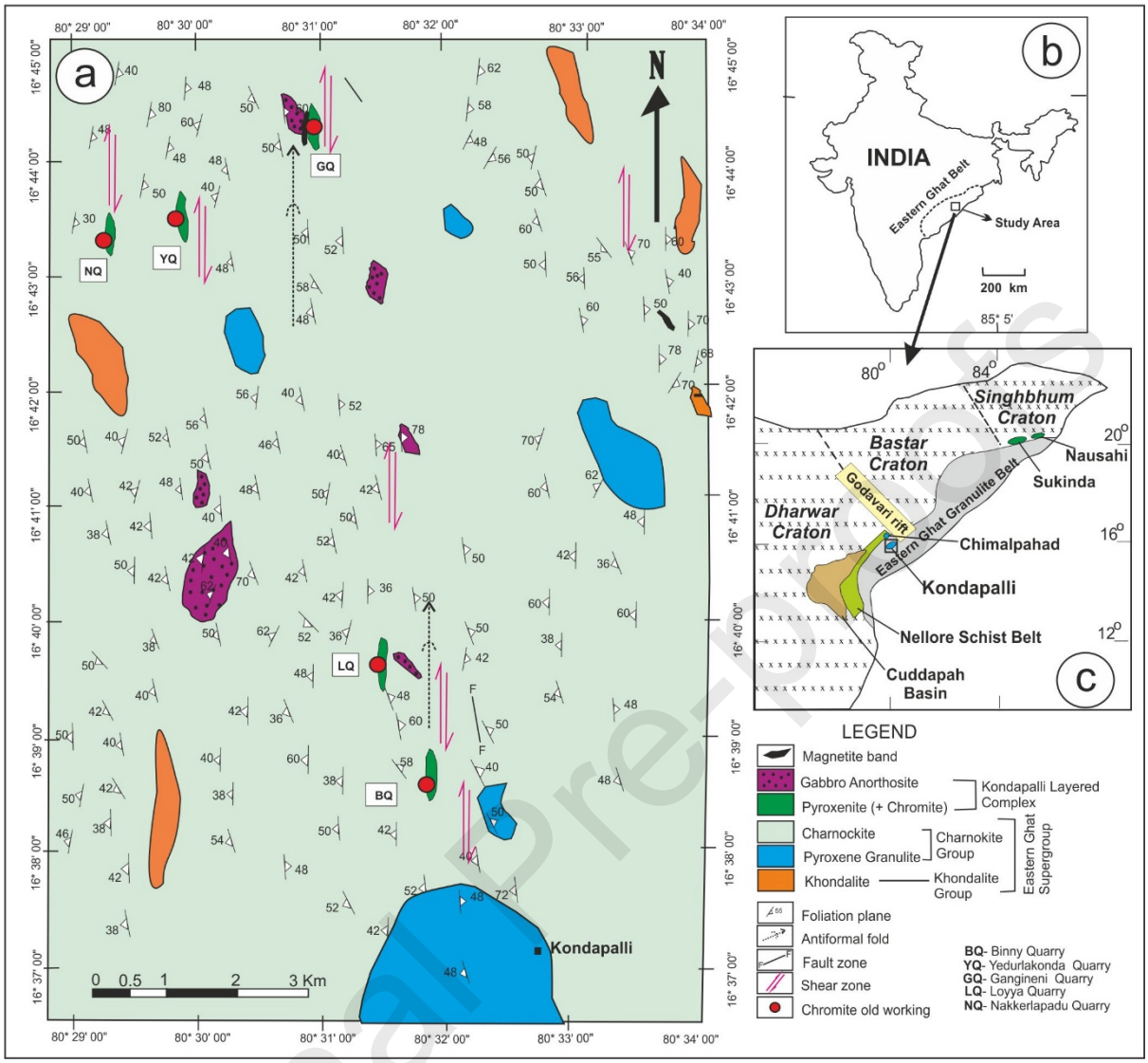

Figure_2

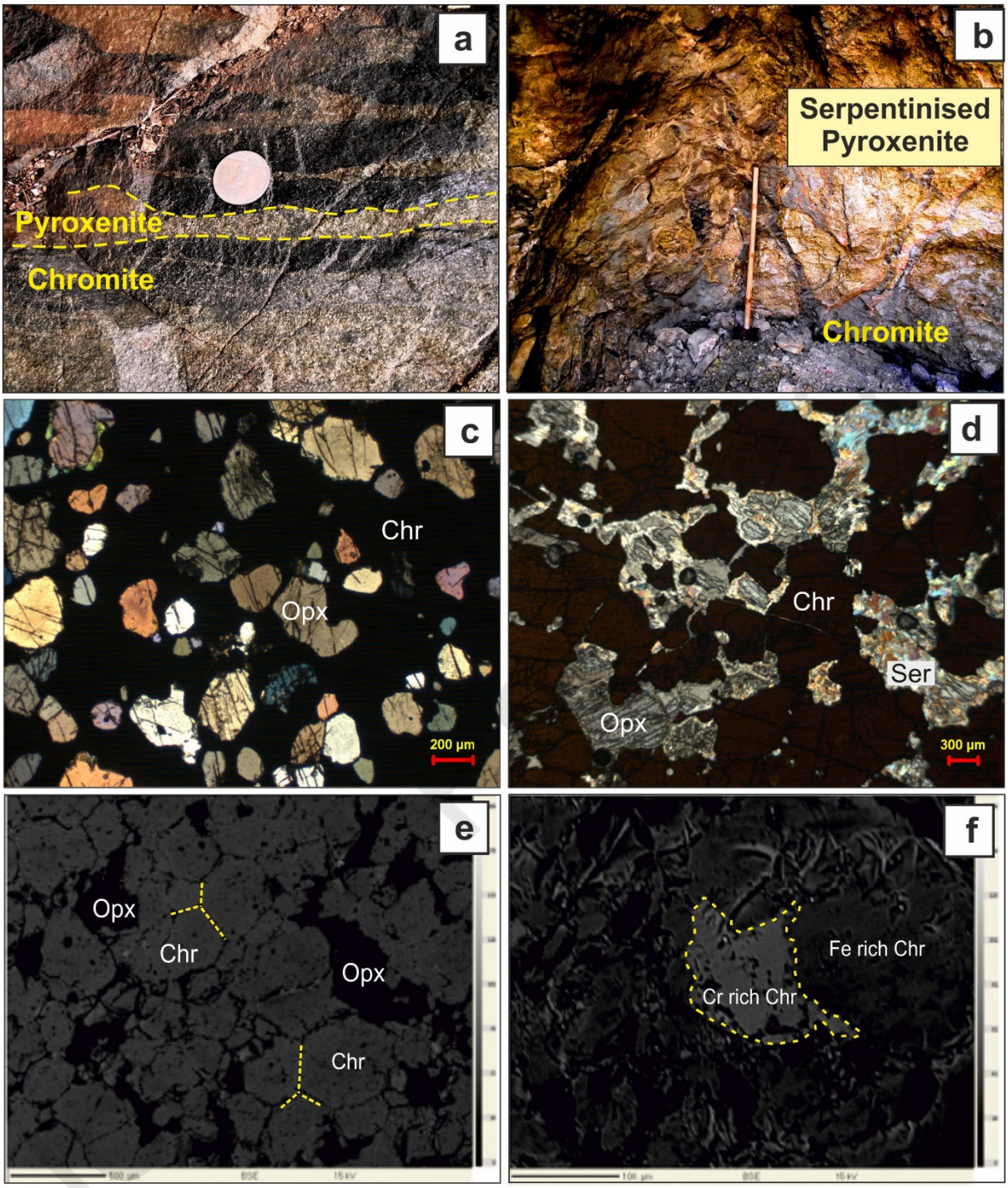
a
Pyroxenite
Chromite
b
Serpentinised Pyroxenite
Chromite
c
Chr
Opx
200 µm
d
Chr
Ser
Opx
300 µm
e
Opx
Chr
Opx
Chr
f
Fe rich Chr
Cr rich Chr

Figure-3a-d

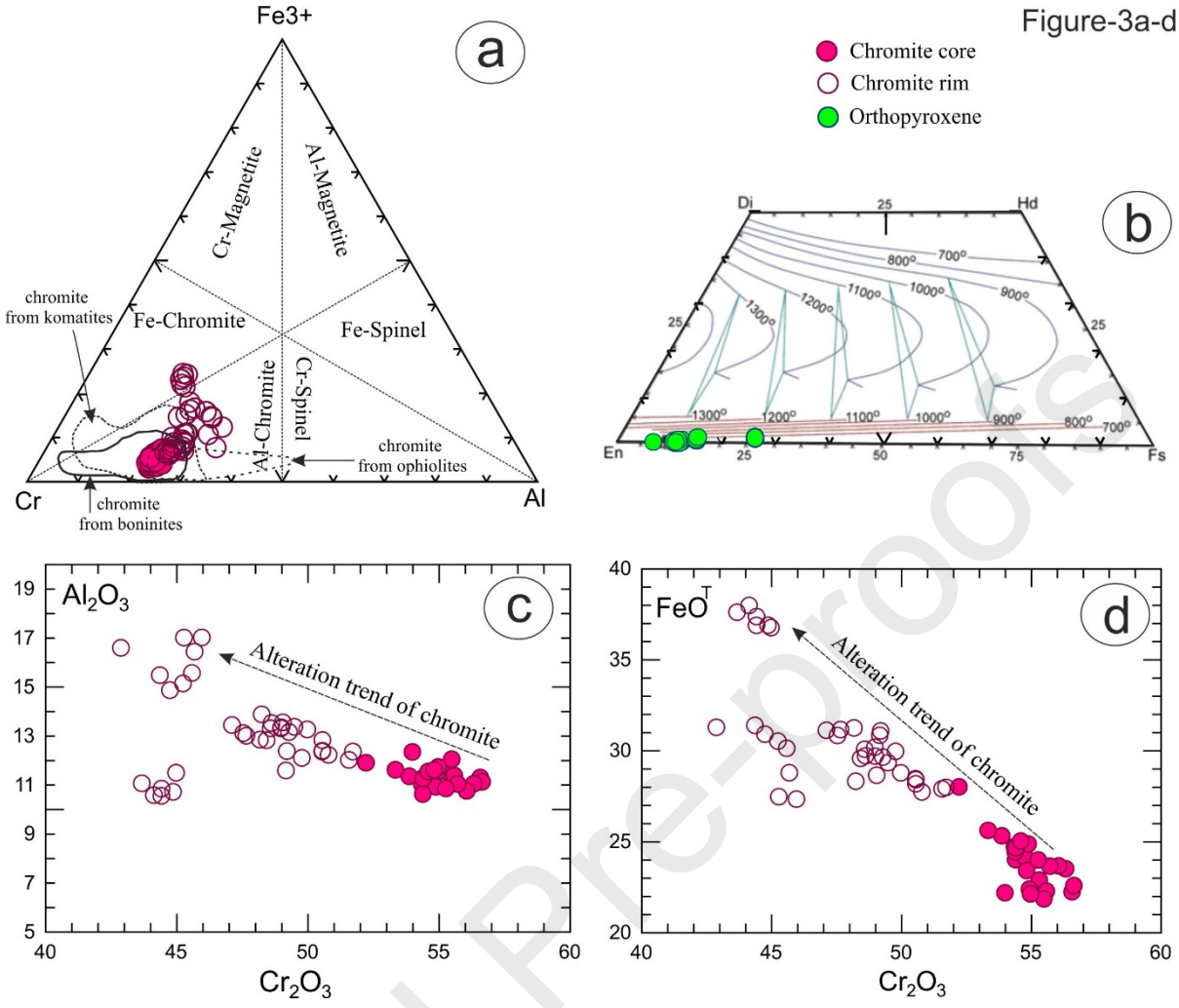

Figure-3e-f

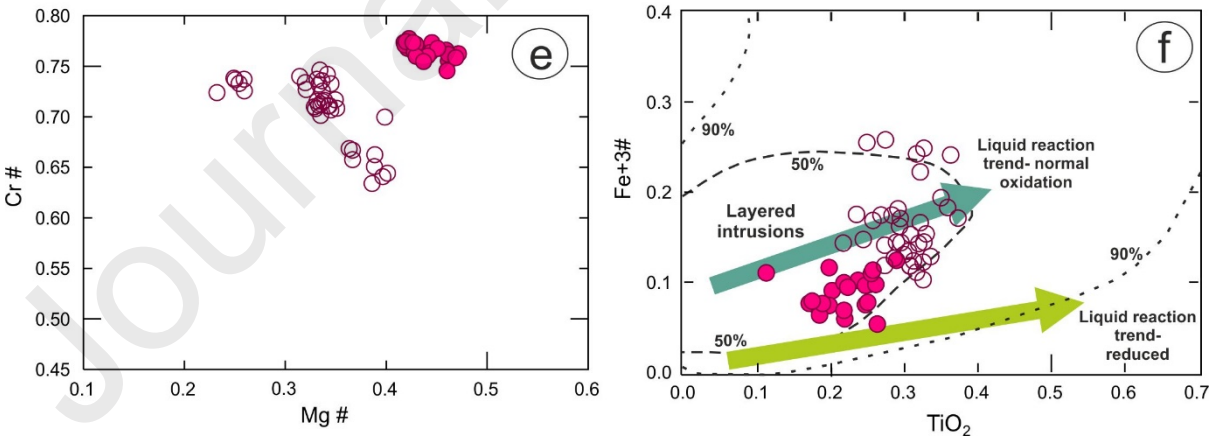

Figure-4

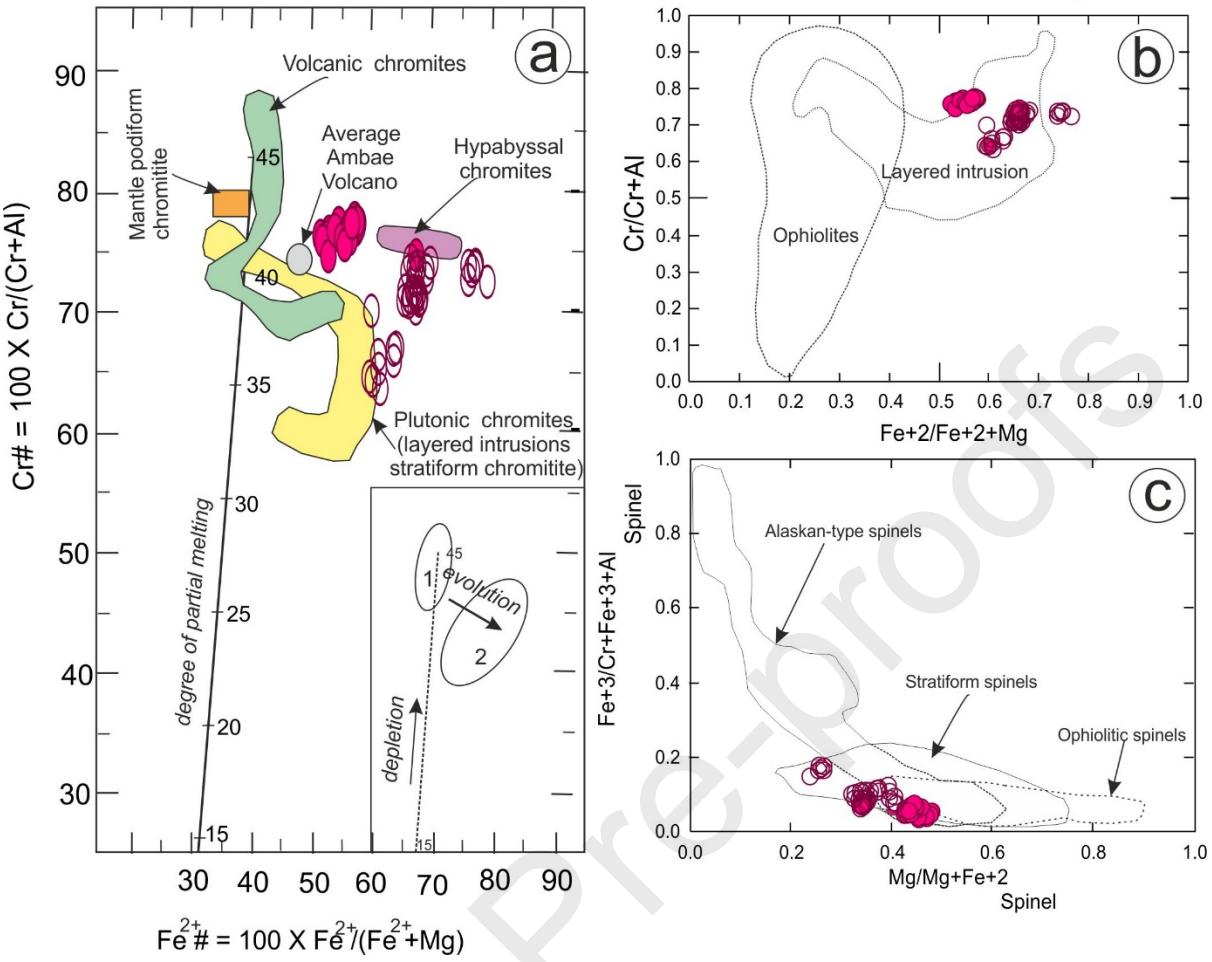

Figure-5

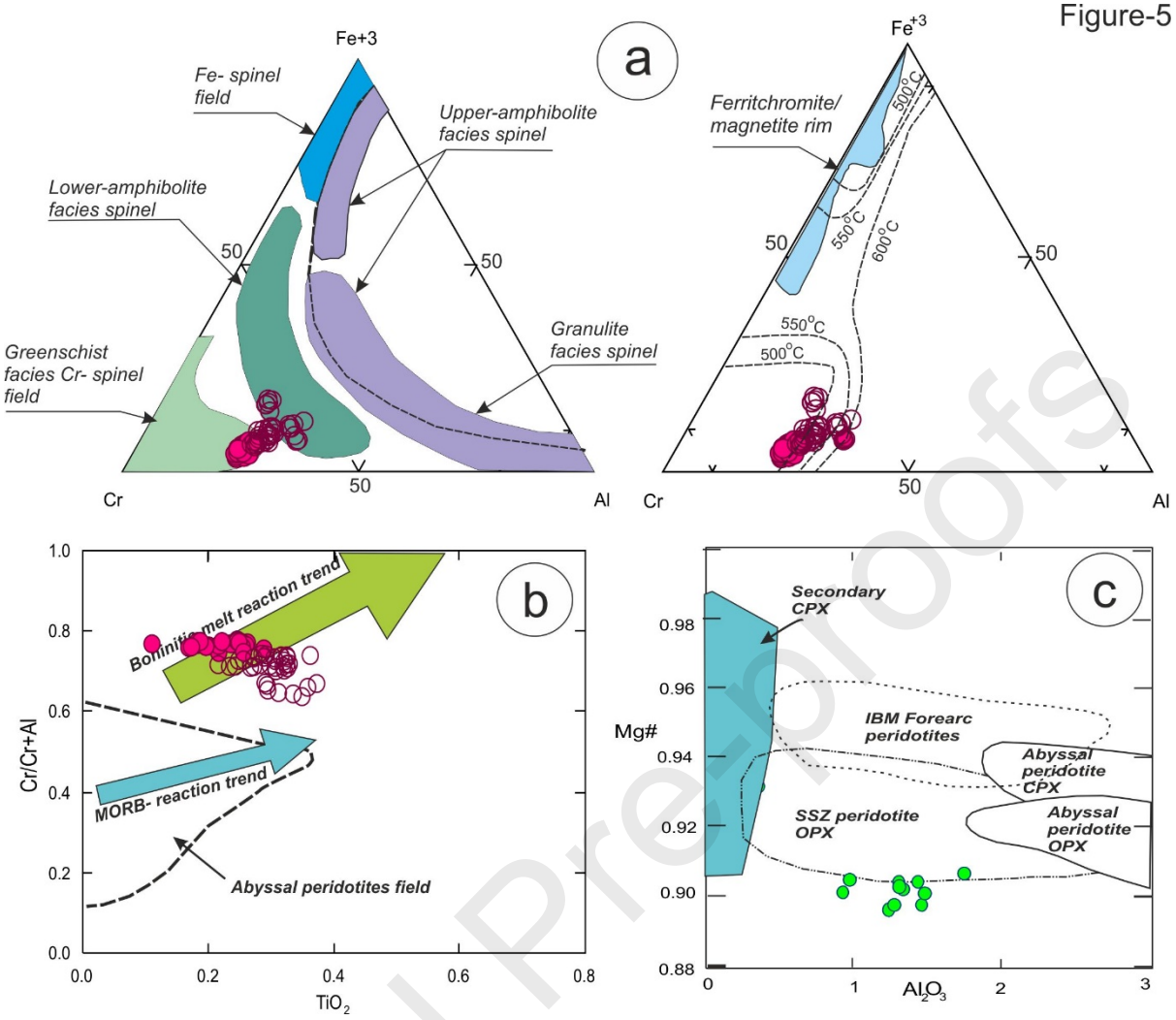

Figure-6

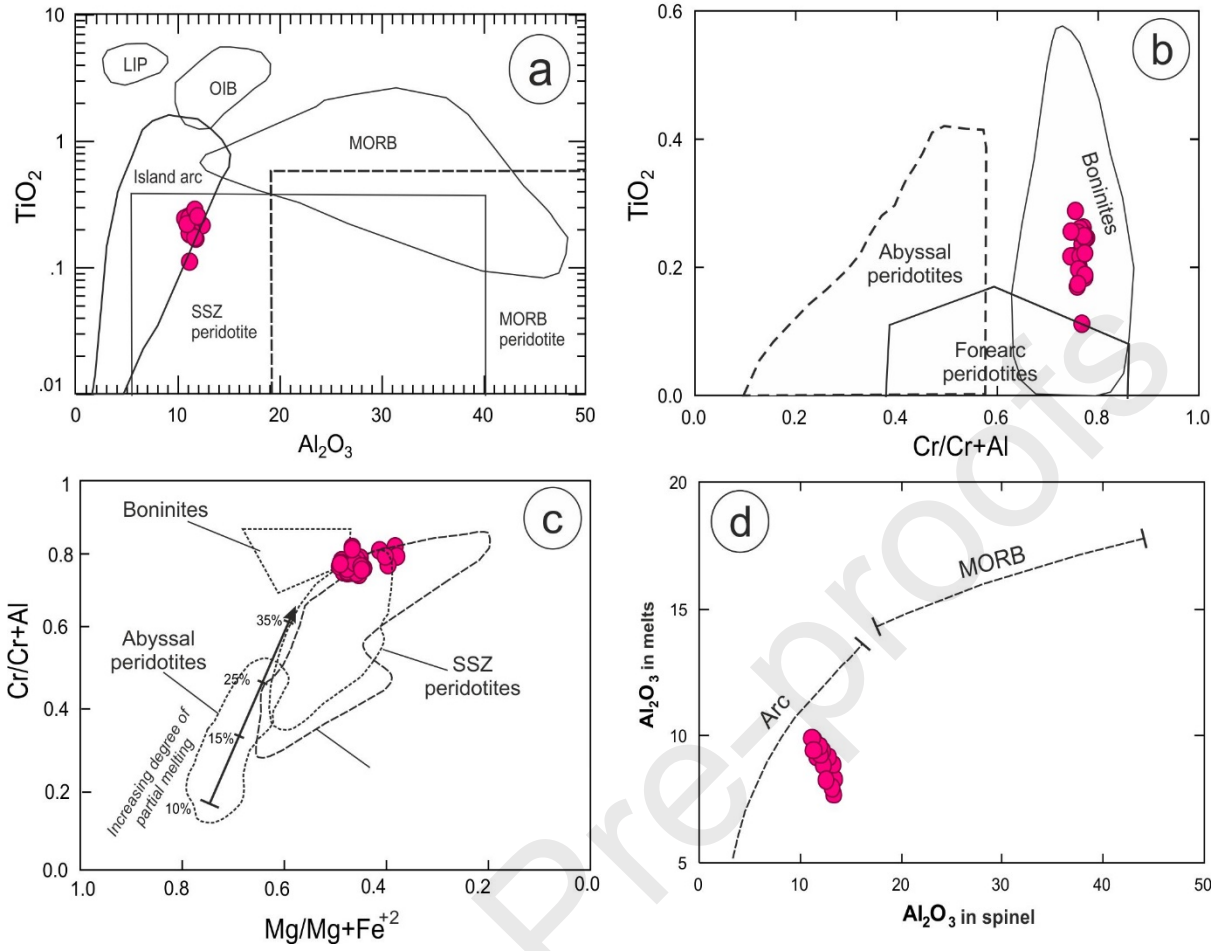

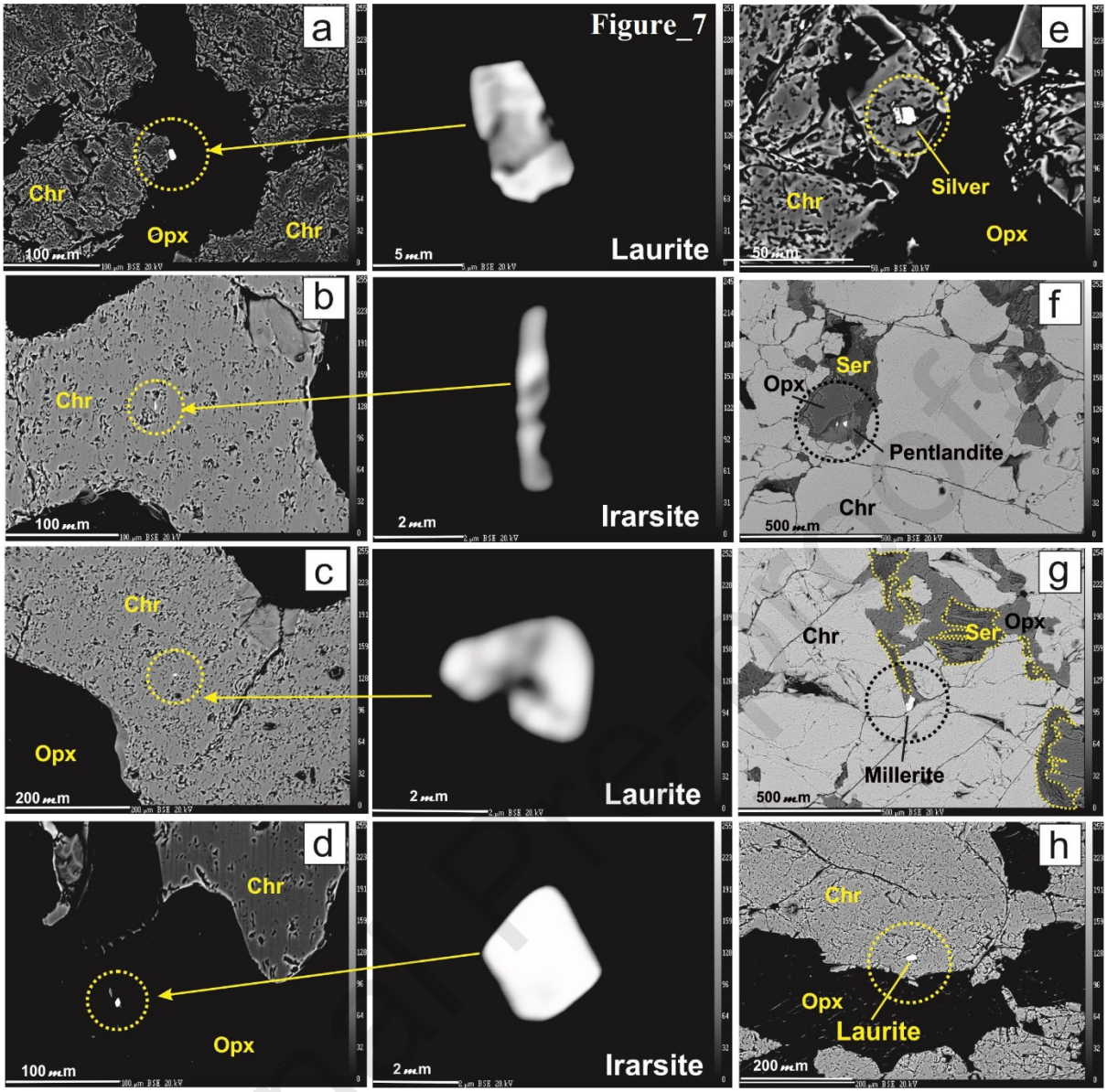

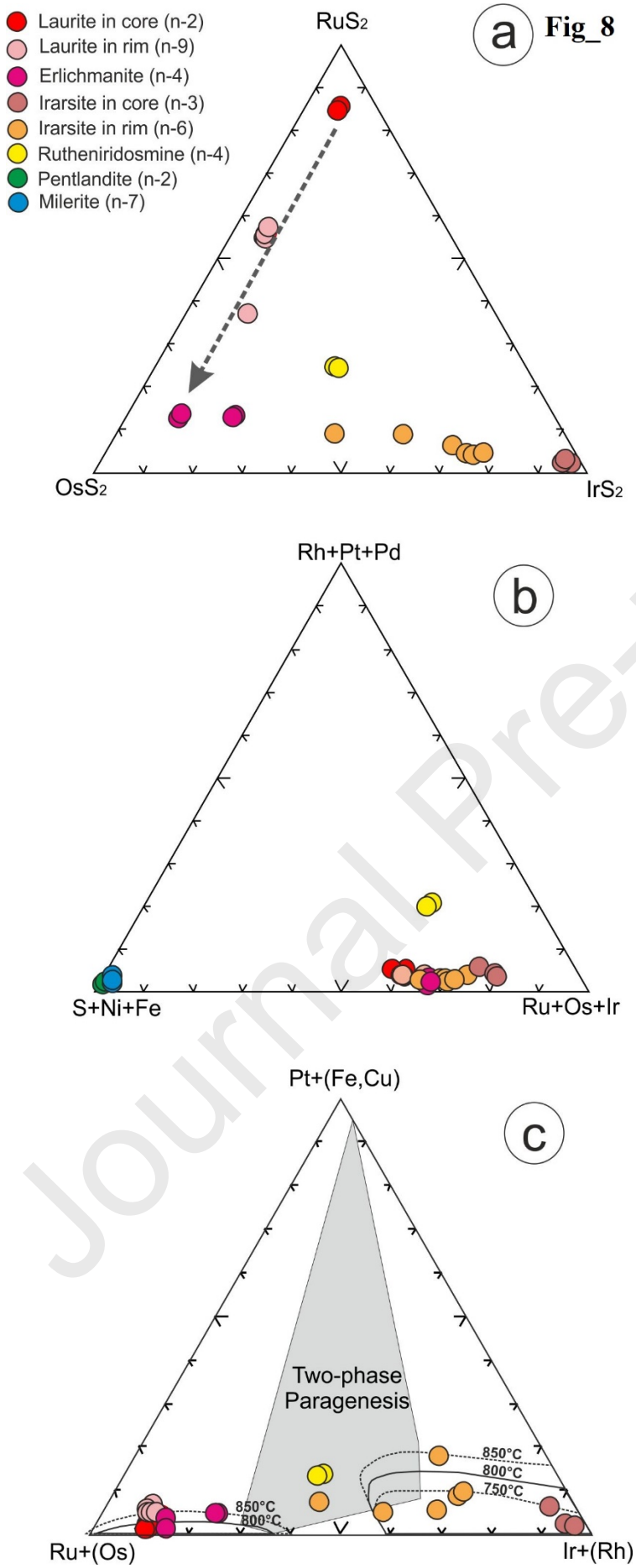

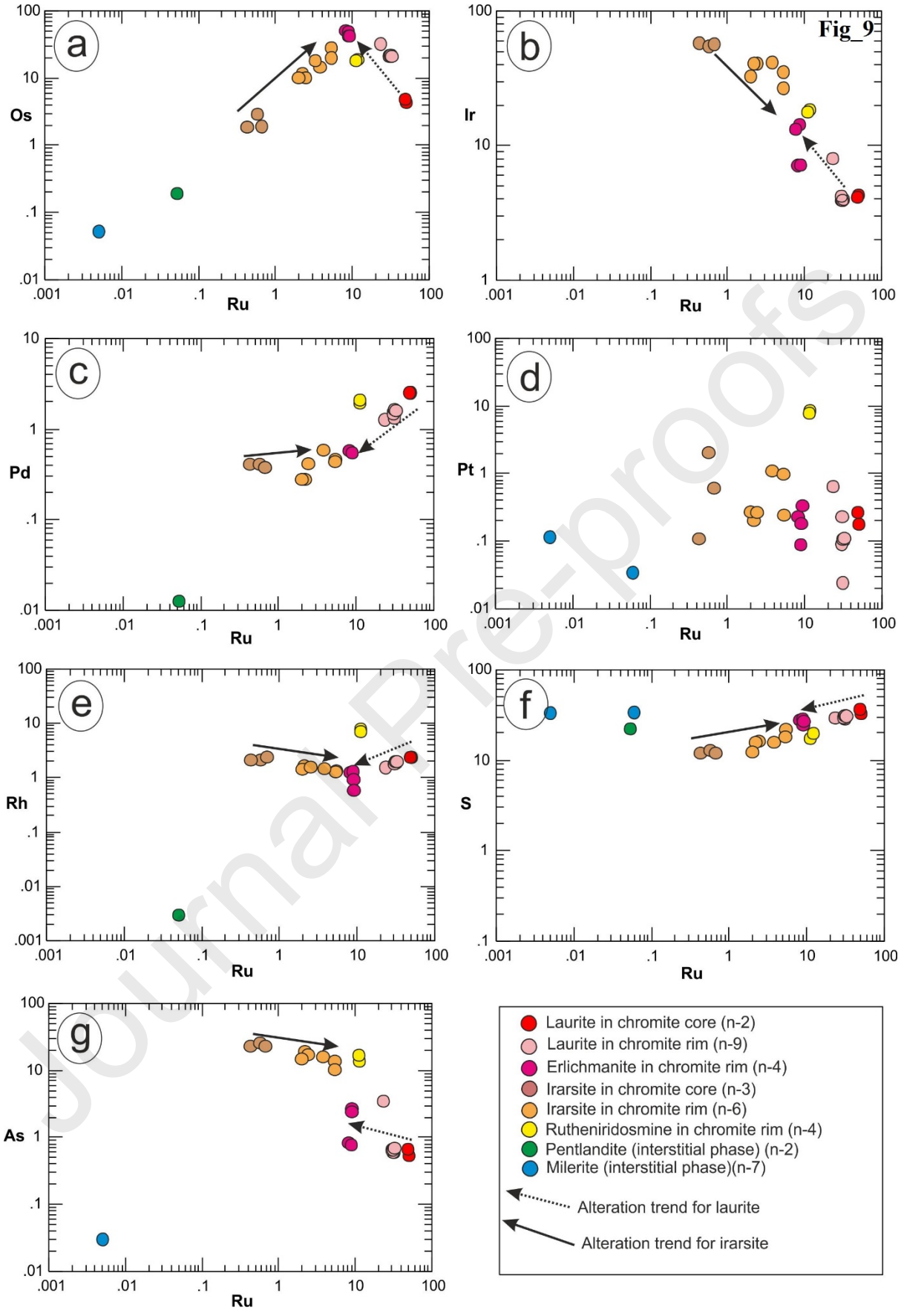

The author stated that there is no conflict of interest from any one regarding the content and data included within the manuscript submitted to OGR

Highlights

1. The textural and compositional variation of chromite and PGM tracks the subtle changes in the magmatic condition during the evolution of KLIC to post-stage alteration.
2. The spinel-core crystallization temperature in the chromitite is estimated to be 500° - 550°C (the spinel stability field was calculated for equilibrium with Fo_{90} olivine), which suggests the core composition is chemically unaltered.
3. Melt calculations suggests parental magma similar to modern primitive boninitic /tholeiitic basalt Chromian spinel chemistry suggests supra-subduction zone-arc tectonic setting Evolution of the Kondapalli arc attributed to the formation of the suture between EDC and EGB.
4. The KLIC form from S-undersaturated boninitic melt with the formation of primary PGM at a higher temperature and low *fS2* i.e, Ru-rich laurite and irarsite. The PGM inclusions within the chromite core are unaffected, while PGM located along rim shows the significant effect of alteration.
5. The PGM assemblage reflects considerable mineralogical reworking. More likely, they represent the product of hydrothermal reworking and remobilization of magmatic PGM. It suggests that PGM integrated the initial magmatic to subsequent secondary imprints during the evolution of KLIC.
6. Primary magma of KLIC is interpreted as less crustally contaminated, mantle-derived arc-related boninites for in an open system.
7. No Ni-Cu-PGE mineralisation is associated with the parent magma of KLIC and it is concluded to be low ranking targets for Ni-Cu-PGE mineralization based on their petrogenesis and tectonic setting of emplacement.